People's Democratic Republic of Algeria
Ministry of Higher Education and Scientific Research

University M'Hamed BOUGARA – Boumerdes

Institute of Electrical and Electronic Engineering
Department of Power and Control

Final Year Project Report Presented in Partial Fulfilment of

the Requirements for the Degree of

MASTER

In Electrical and Electronic Engineering

Option: **Power Engineering**

Title:

Photovoltaic Cell I-V and P-V Characteristics: Simulation versus Measurement

Presented By:

Touabi Cilina

Supervisor:

Pr. Bentarzi Hamid

Abstract

Among all renewable energy sources, solar energy has acquired the highest growth rate worldwide in the last years. The major application of solar energy is photovoltaic (PV) power generation. For an accurate study in different PV applications, it is very important to model the basic device of the PV cell. However, the model parameters are usually unavailable in the datasheet provided by the manufacturers and their values change over time due to the PV degradation. Thus, how to estimate appropriate parameters is of high importance. This work presents two methods for identifying the optimal parameters of a PV generating unit. In both methods the PV generator is simulated using the one diode model. The first method is based on grey wolf algorithm where the parameters of the model are identified using only datasheets provided my manufacturers, this algorithm is included in a SIMULINK simulation for constructing the I-V and P-V characteristics. The second method is based on an opposition-based particle swarm optimization algorithm where the objective function is derived from the experimental current-voltage data. These approaches are found to be useful for designers since they are simple, fast and provide accurate results. The analysis is performed on various PV modules under different environmental conditions. The final results are compared and discussed to demonstrate the efficiency and accuracy of the proposed work.

Dedication

I dedicate this work to the person who believed in me my mother.

To my father who taught me the importance of hard work

To my sisters Dihia and Louiza,and my brother Lounis To my grandparents who loved me and always supported me

To all my family and friends who helped me and made me a better person

Cilina TOUABI

Acknowledgments

Praise to Allah, the supreme for leading me in my study path, and for giving me the will and patience that allowed me to complete this work.

This project was realized at the Institute of Electrical and Electronics Engineering at the University of Boumerdes and was accomplished under the supervision of Pr. Bentarzi.
I would like to express my deep gratitude and warm thanks to my supervisor who have guided and oriented me throughout the achievement of this work. Furthermore, I extend my thanks to all teachers who have done their best to transmit their knowledge.

Very special thanks are to my parents and my family for their love, motivation and support through my academic years.

Finally, I acknowledge with much appreciation the jury members for having honored me by agreeing to evaluate this work.

Table of Contents

List of Abbreviations

Abbreviation	Definition
AC	Alternative Current
AM	Air Mass
ABC	Artificial Bee Colony
CdTe	Cadmium Telluride
CSP	Concentrated Solar Power
CPSO	Chaos Particle Swarm Optimization
CSA	Cuckoo Search Algorithm
CIABC	Chaotic Improved Artificial Bee Colony
CARO	Chaotic Asexual Reproduction Optimization
DC	Direct Current
DDM	Double Diode Model
GaAs	Gallium Arsenide
GWO	Grey Wolf Optimization
IOB-PSO	Improved Opposition Based Particle Swarm Optimization
ImCSA	Improved Cuckoo Search Algorithm
MENA	Middle East and North Africa
MATLAB	Matrix laboratory
N	Negative
NOCT	Nominal Operating Condition Temperature
NR	Newton Raphson
NRMSE	Normalized root mean square error
ODM	One Diode Model
PV	Photo-voltaic
P	Positive
PSO	Particle Swarm Optimization
PS	Pattern Search
RMSE	Root mean square error
STC	Standard Test Conditions
SA	Simulated Annealing
TDM	Three Diode Model

List of Symbols

Symbol	Description	Unit
I	Current	A
V	Voltage	V
P	Power	W
I_{ph}	Photo current	A
n	Diode Ideality factor	-
I_s	Reverse Saturation Current	A
R_{sh}	Shunt resistance	Ω
R_s	Series resistance	Ω
η	Efficiency	-
T	Temperature	°c
G	Irradiance	w/m^2
V_{oc}	Open circuit voltage	V
I_{sc}	Short circuit current	A
V_{mpp}	Voltage at maximum power point	V
I_{mpp}	Current at maximum power point	A
Pmax	Maximum power	W
Pin	Input power	W
I_d	Diode current	A
I_{sh}	Shunt resistance current	A
V_t	Thermal voltage	V
K	Boltzmann's constant	J/K
q	Elementary charge	C
α	Alpha	-
β	Beta	-
δ	Delta	-
ω	Omega	-
N_s	Number of series connected cells	-
K_i	Temperature coefficient of I_{sc}	-
K_v	Temperature coefficient of V_{oc}	-
c1	Cognitive factor	-
c2	Social factor	-
w	Inertia weight	-

List of Figures

List of Tables

CHAPTER ONE:

Introduction

1.1 Framework

Electricity expansion in the 21st century has led to a fast technological, economic and social development, from which an extreme dependency on electricity was born. Electricity is currently a utility, and this fact has caused quite a lot of discussion in the recent decades, due to the consequences of its generalized use and mass exploitation of the primary energy resources used for its generation. Energy supply is currently one of the biggest problems that the human development is facing as the world's electricity production is based mainly in the fossil fuels exploitation and the energy consumption is increasing [1]. The intensive use of fossil fuels leads to large greenhouse gases emissions, and thus to a global warming increase, which has consequences such as average sea level increase, extinction of animals and plants and changes on the intensity of rain. In response to this problem, renewable energies technologies have arisen, powered by renewable sources, as the solar energy, wind, biomass and biofuels and sea waves and tides.

Solar energy is recognized as the most promising alternative to the conventional energy sources [2], and many scientists believe that the sun is the source that will permit to ensure a greener future for the planet. The solar radiation intensity, which reaches earth surface directly, is approximately 1360 W/m2 [3]. So, earth surface receives solar energy equal to 3400 000 EJ/year. By comparing this energy to global energy consumptions, it becomes 7500 times more than the world's total annual primary energy consumption of 450 EJ [4]. If this available energy or even a part of it can be harnessed, the global energy problems, then, could be solved.

The major application of solar energy is photovoltaic (PV) power generation, which has a growth of more than 22% in 2019 and predicted to be over 720 TWh [6]. The PV systems are easy to install, noise-free, and can directly convert solar energy to electrical energy. Furthermore, the fact that PV installation can operate for 30 years or even more with little maintenance reduces its operating costs and makes it insignificant comparing to existing power technologies. The total worldwide installed capacity of the photovoltaic technology was by the end of 2019 an amounted value of 580.159 GW [7].

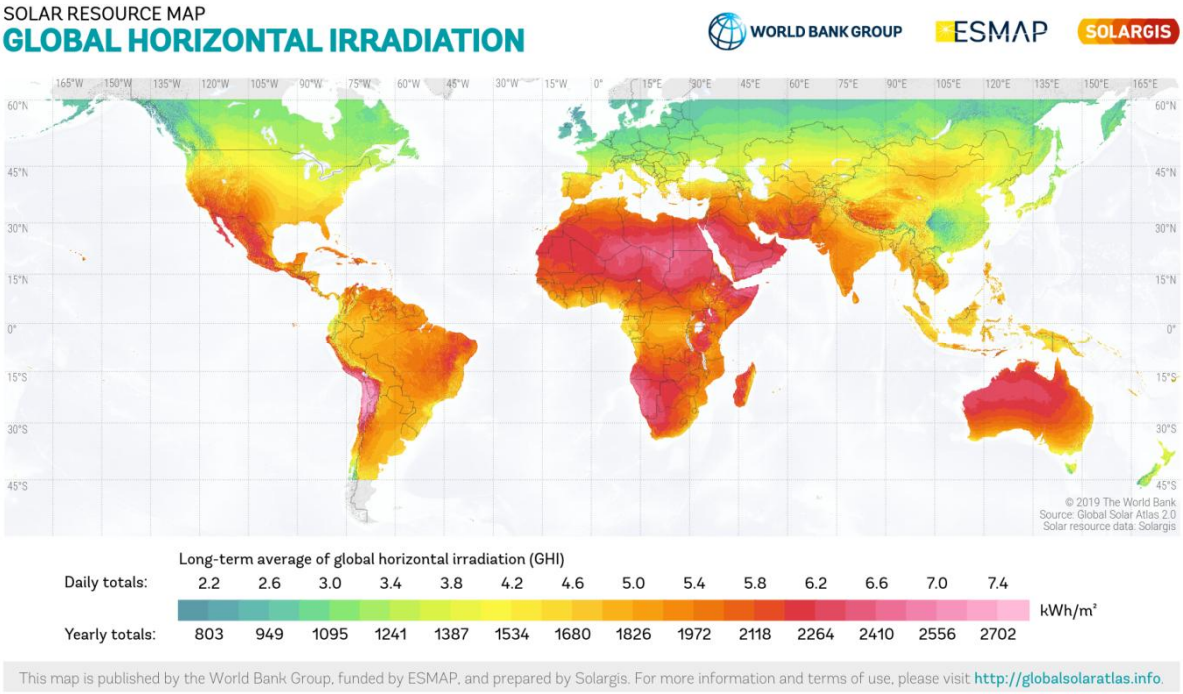

Figure 1.1 Global horizontal irradiation distribution [kWh/m^2] [5].

1.2 Problem Formulation

The photovoltaic (PV) power is provided after the conversion of sunlight into electricity by means of semiconducting materials that exhibit the photovoltaic effect. This conversion is done at the level of a basic elementary device of PV system which is the PV cell. The performance of photovoltaic systems is entirely dependent on the working condition they are established in. The electrical output is subject to variations due to the fluctuating temperature and irradiance that depend on the season and location conditions. Therefore, researchers worked on developing suitable models for photovoltaic (PV) cells and modules to simulate and forecast their behaviour under different circumstances, which is central to the design, manufacturing, and evaluation of PV systems. Also, an accurate estimation of the models' parameters is at the heart of the reliability of each model. However, the model parameters are usually unavailable in the datasheet provided by the manufacturers and their values change over time due to the PV degradation. Thus, how to estimate appropriate parameters is of high importance, and has been highly attracted by researchers. The one diode model (ODM) is considered as the most suitable model used to characterize the solar cells/modules [8] in comparison to the double diode model (DDM) and the three-diode model (TDM) as it has a

minimum number of parameters and a good level of accuracy. The five electrical parameters of the ODM are: photocurrent (I_{ph}), diode ideality factor (n), reverse saturation current (I_s), shunt resistance (R_{sh}) and series resistance (R_s).

Several methods have been developed to extract the ODM parameters which are classified into three main categories:

- Numerical methods.
- Analytical methods.
- Artificial intelligence or optimization methods.

Numerical methods are widely used since they provide a good compromise between speed of calculation, simplicity, and accuracy. These approaches utilize numerical methods to solve a system of a few non-linear equations related with the PV cell. However, optimization methods are proved to be very efficient for handling difficult optimization problems that are large, complex, non-linear and multimodal and provide more accurate results.

1.3 Motivation

The public authorities in Algeria tend to give an important support to the sector of development of renewable energies to replace the fossil fuels energy whose resources are increasingly running out, and meet the energy demand.

Algeria has the highest technical and economic potential for solar power exploitation in the MENA region, with about 170 TWh per year. First industrial scale solar thermal power project has been initiated by inauguration of HassiR'Mel power station in 2011. This new hybrid power plant combines a 25 –megawatt (MW) concentrating solar power array in conjunction with a 130 MW combined cycle gas turbine plant. Furthermore, Algeria has launched in 2011 a national program to develop renewable energy based on photovoltaic (PV), concentrated solar power (CSP) and wind power, and to promote energy efficiency. The program consists of installing up to 12 GW of power generating capacity from renewable source to meet the domestic electricity demand by 2030. [9]

The following figure shows the national renewable energy program in Algeria (2015 - 2030).

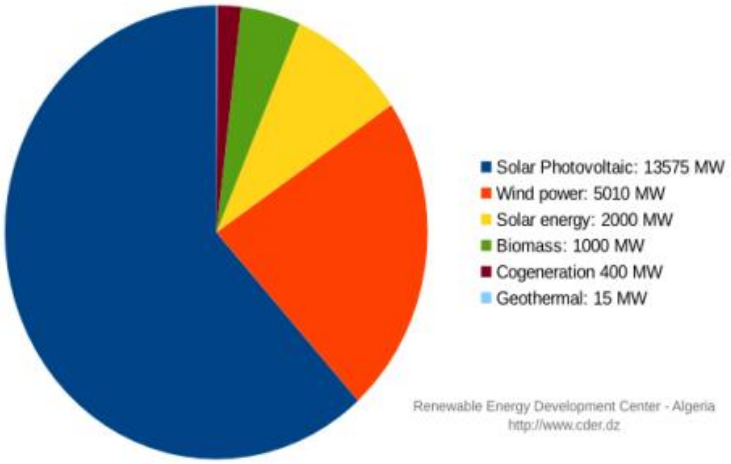

Figure 1.2 Renewable energy development in Algeria (2015-2030) [10].

1.4 Objectives

In this project, our interest is to:

1) Simulate the I-V and P-V Characteristics using one diode model (ODM) associated with a developed algorithm that permits finding the appropriate value of the needed parameters simply from datasheet information provided by the manufacturer.
2) Simulate the I-V and P-V Characteristics under different operational conditions for comparison study purpose.
3) Develop an algorithm for ODM parameters identification from measured I-V data.

1.5 Structure of dissertation

- The first chapter is intended as an introduction to the subject, it discussed the importance of renewable energy sources, especially, solar energy. It gave a brief background about the Photovoltaic power generation and the challenges facing this technology.
- Chapter two is an overall background on photovoltaic system principle, construction, and characteristics. It discussed the effect of the changing environmental conditions on PV cells parameters. Moreover, this chapter set the various advantages of PV technology.
- Chapter three covers the modelling of PV cells based on one diode model, it consider the effect of some model parameters. Furthermore, the PV parameters identification

methods are discussed and two algorithms are presented: one for parameters identification based on datasheet information, this algorithm is included in a developed PV model simulation for extraction of I-V and P-V characteristics; the second algorithm is developed for model parameters identification from experimental I-V data.

- Chapter four presents the results obtained from the developed simulation and the proposed algorithms under different working conditions. These results are compared and discussed to demonstrate the efficiency and accuracy of the proposed work.
- The last chapter is intended as a general conclusion for the proposed work. Furthermore, it presented perspectives for enhancing any possible future work.

CHAPTER TWO:

Photovoltaic System Principles

2.1 Photovoltaic

Photovoltaic is a word composed of photo which means light and voltaic which stands for voltage. Photovoltaic (abbreviated PV) is the most direct way to convert solar radiation into electricity. Photovoltaic or solar cells are semiconductor devices that transform sunlight into direct current (DC) electricity. PV cells are arranged in modules and arrays, and can be used to charge batteries, operate motors and to a power to any electric loads; from small electronics like calculators up to homes appliances. PV systems are also able to produce alternating current (AC) if they are equipped with the power conversion equipment, inverters.

2.2 Photovoltaic Cells

2.2.1 Structure

A solar cell (also known as PV cell) is an electrical device that converts light energy into electrical energy through the photovoltaic effect . It is basically a p-n junction diode.

Photovoltaic cells are made of two or more thin layers of semi-conducting material, generally silicon.. When exposed to solar radiation the semiconductor generates electrical charges which can be conducted away by metal contacts as direct current (DC).

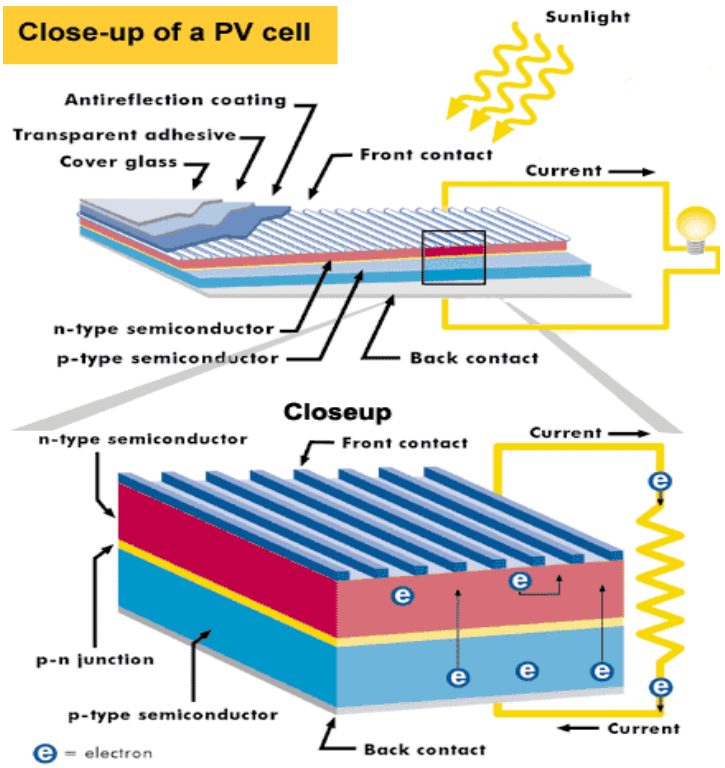

Figure2.1. PV cell construction

2.2.2 Materials Used In PV Cell

There are different types of solar cells available commercially: one is thin film solar cells and second is crystalline silicon solar cells.

i. **Crystalline materials**

Crystalline silicon cells can be sub-categorized as:

- Mono-crystalline Silicon:
  In this type, each cell has a single crystal and it is much efficient (η= 15%) than other crystalline cells due to good electrical, physical and chemical characteristics of silicon. These cells are very expensive.
- Polycrystalline Silicon:
  The polycrystalline silicon cells are better than mono-crystalline silicon cells in respect of simpler and cost efficient manufacturing process. In this type, each cell has more than one crystal. These cells are less efficient that mono-crystalline silicon cells (η= 12%).

ii. **Thin film materials**

In these cells, semiconductor films are very thin which are deposited on low cost substrate like glass, metal or plastic. Hence, it is less expensive but its efficiency is also lower than other types of PV cells. The light absorbing material requirements are reduced from these cells. Many types of thin film materials are available.

- Amorphous silicon
  Such type of materials is highly defective even with hydrogenation, resulting in low lifetime of minority carrier and less conversion efficiency (η= 6%). These materials can be manufactured on low temperatures and less energy. Hence, they are cost effective in manufacturing. The performance of such materials degrades when they are exposed to sun, which is their major drawback.
- Cadmium Telluride (CdTe)
  The materials cadmium and tellurium are used to form a poly-crystalline compound. During manufacturing of PV cells, cadmium telluride is usually sandwiched with cadmium sulphide. Among all thin film technologies, this CdTe poly-crystalline

compound has the lowest production cost. In this technology, the substrate used is sodalime glass (low cost).

- Copper Indium Selenide

  Such type of compound semiconductor material is composed of indium, selenium and copper. The material copper indium selenide is a firm solution and unlike amorphous silicon, this compound made solar cell that does not degrade under light intensity. However, it is much costly due to its complex manufacturing process.

- Gallium Arsenide (GaAs)

  Gallium and arsenic materials are used to form this semiconductor compound.

  GaAs is much efficient than silicon but it is also much expensive. It is used in many applications like space, concentrator systems etc.

2.3 Principle of Photovoltaic

A PV cell is basically a semiconductor diode as shown in Figure 2.2. Working on the principle theory of photoelectric effect which is defined as, any material exposed to light generates charge carriers, when sunlight that is basically photons of different frequencies and energies, hits the solar cell surface and is absorbed by a semiconducting material, such as silicon, electrons will be excited from atoms, making them free and ready to move.

Each material has band gap between conduction and valence bands and electrons goes into conduction bands when the energy of incident photon becomes greater than band gap energy. That means, not all photons which hit the surface of the PV cell are converted to electricity. Only photons with enough energy, related to their wavelengths, are able to free an electron-hole in the semiconductor of PV cell. As such, photons with less or excess of required energy will result in heat. This contributes in the low efficiency of Photovoltaic.

The structure of PV cell makes the electrons to move in a single direction. In the same time freeing electron is accompanied by creation of holes, positive charges which flow in the opposite direction to the electrons.

In order to avoid recombination of produced hole – electron pairs and separate between them, the PV cell is made of two semiconductors, P-and N-materials .Those are created by an impurity addition into the semiconductor crystal. Due to the doping, the N-region contains an excess of free electrons, while the P region have a lack of them, and each missing electron is considered as a “hole”. Joining of these two materials will result in a p-n junction and due to

the differences in concentration at the junction between the two regions, electrons diffuse into the p-region and "holes" into the n-region, therefore an electrical field in the formerly electrical neutral junction comes into existence. The established electric field acts as a diode and allows electrons to flow only in one direction. This movement of electrons results in current that flows in the opposite direction.

Free electrons then flow through the material and are collected by the metal plates that are usually deposited on bottom and top of PV cells, producing then electricity.

Hence, band gap energy corresponds to threshold energy which in turn gives threshold frequency of a semiconductor material. In photovoltaic material, photoelectric emission rate can be increased by increasing light intensity.

Solar cell produces electricity with very small voltage; for the common single junction silicon solar cell it is approximately about 0.5 to 0.6 volts. Due to this, they are available in the form of modules or panels to provide sufficient voltage and current for real life applications; as shown in the next section.

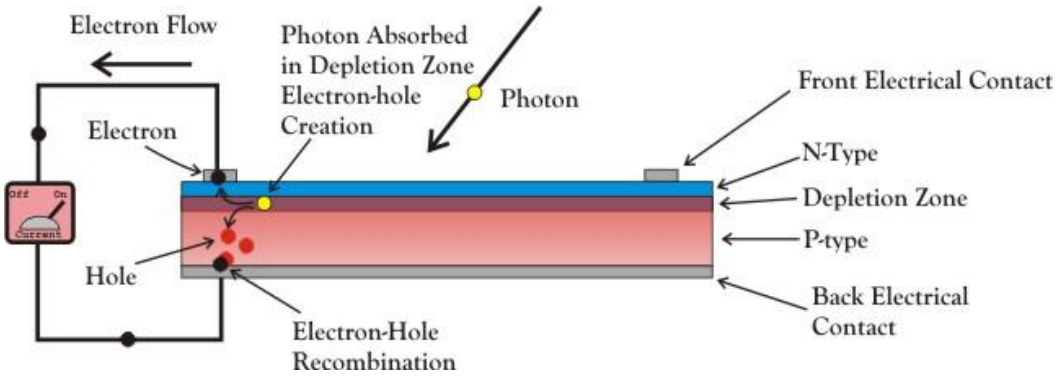

Figure 2.2. Photo electric effect of PV cell

2.4 PV Cells, Modules and Arrays

Typically, a photovoltaic cell gives voltage between 0.5 and 0.8 V at its output. This output voltage depends on the semiconductor material. Each PV cell power production is very low, so numbers of photovoltaic cells are used in series to make a photovoltaic module as shown in Figure 2.3. Commercially available photovoltaic modules have 36 or more PV cells joined in series. Photovoltaic modules are joined in parallel and series to make PV arrays. So, PV cells are either connected in series to add voltages of each cell with same current (for high voltage

requirement) or connected in parallel to add current passing through each PV cell with same voltage (for high current requirement) to get desired power.

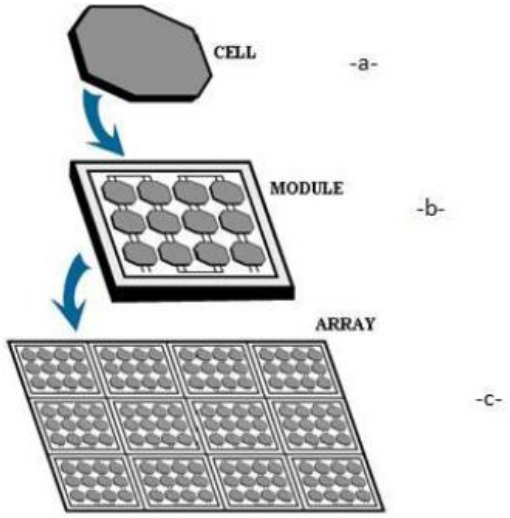

Figure 2.3. a) cell b) module c) array

2.5 Characteristics Of A PV Cell

Electrical characteristics of PV modules are given by the producers under precise conditions that are known as standard test conditions (STC). Such conditions are defined by the ambient temperature $T_{STC} = 25°C$, irradiation level $G_{STC} = 1000\ W/m^2$, and the air mass value AM=1.5. However, in the working field, PV modules operate at higher temperatures and somewhat lower insulation conditions. In order to determine the power output of the solar cell, it is important to determine the expected operating temperature of the PV module. The nominal operating cell temperature (NOCT) is defined as the temperature reached by open circuited cells in a module under the conditions: solar irradiance G = 800 w/m^2, air temperature $T_{ambiant}$= 20°c and wind speed =1m/s .Then the cell temperature can be calculated by equation (2.1)

$$T_{cell} = T_{ambiant} + \left(\frac{NOCT-20}{800}\right) * G \qquad (2.1)$$

Where G is taken in [w/m^2]

i. I-V and P-V Curves

Solar cell I-V curve characteristic curve of a particular PV cell ,module, or array shows the possible combinations of its current (I) and voltage (V) outputs. Similarly, the P-V curve shows the possible combinations of its power (P) and voltage (V) outputs. In DC electrical circuits, the power is the product of the voltage and the current, as shown in equation (2.2)

$$\mathrm{P(Watts)} = \mathrm{I(Amperes)} * \mathrm{V(Volts)} \tag{2.2}$$

The typical I-V and P-V Characteristics of a photovoltaic cell are shown in Figure 2.4. The main three significant parameters on the photovoltaic characteristics are open circuit voltage (V_{oc}), short circuit current (I_{sc}) and maximum power point (V_{mpp}, I_{mpp}).

- The Maximum current in photovoltaic cell is produced when there is a short circuit between its positive and negative terminals and it is denoted as I_{sc}. As $I=I_{sc}$ the voltage in the circuit is zero.
- The maximum voltage, denoted as V_{oc} occurs when there is a break in the circuit. Under this condition, no current flows in the circuit and resistance is infinitely high, since the circuit is deficient. Typical value of the open-circuit voltage is located about 0.5 and 0.6 V for Crystalline Cells and between 0.6 and 0.9 V for Amorphous Cells.
- The maximum power achieved from a photovoltaic cell occurs at a point on the bend in the I-V curve known as the maximum power point (MPP). The voltage and current at this Point are designated as $V_{mpp}$and I_{mpp}.

Generally, these parameters are provided in the datasheet by manufacturers of a particular photovoltaic cell or module. When the PV cell is connected to an external load, the electrical characteristics of the load determine the actual point on the I-V curve at which the photovoltaic cell operates. PV cells are often connected to the load through a maximum power point tracker (MPPT) which regulates cell voltage so that cell operates at maximum power point. I-V curve shape is same and does not change for module or array of photovoltaic cells but it is scaled depending on number of cells joined together. Environmental parameters such as ambient and cell temperatures, irradiance, wind speed and dust affects the shape by disturbing the maximum power points on I-V curve.

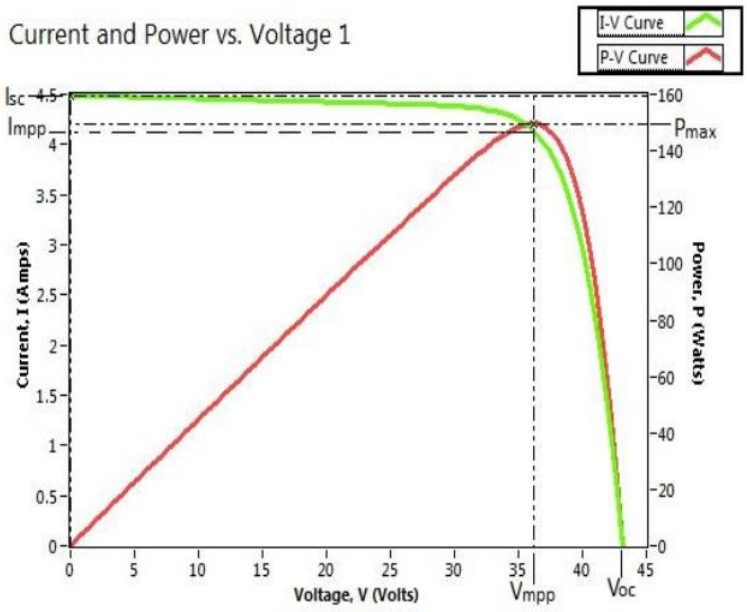

Figure 2.4. I-V and P-V characteristics of PV cell

ii. The Fill Factor

One more essential parameter of the photovoltaic characteristics is known as the Fill Factor (FF). It is a parameter that basically determines the quality of the solar cell by determining the maximum power that can be produced, in conjunction with open circuit voltage and short circuit current.

Graphically, the FF is a measure of the "squareness" of the solar cell. It is the area of the largest rectangle fitting in the IV curve. The fill factor is illustrated in the following Figure 2.5 The closer the fill factor value is to the unity, the greater is the efficiency of the PV cell.

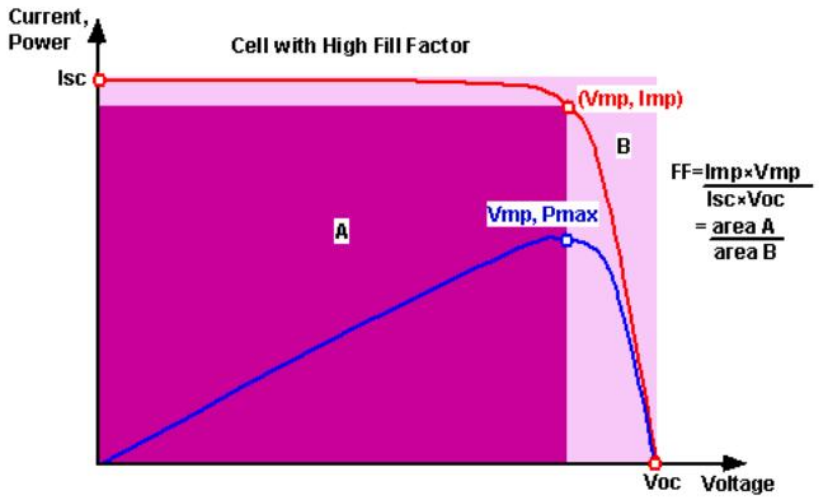

Figure2.5. -Cell output current (red line) –Power output (blue line) –FF graphically

The fill factor can be determined using the following equation (2.3):

$$FF = \frac{V_{mpp} * I_{mpp}}{V_{oc} * I_{sc}} \quad (2.3)$$

iii. Efficiency

Efficiency is used to judge the performance of a solar cell. It is the ratio of the output energy from the solar cell to the input energy from the sun. It highly depends on the conditions under which it is measured (intensity of the incident sunlight, temperature).

It is defined as:

$$\eta = \frac{P_{max}}{P_{in}} \quad (2.4)$$

2.6 Effect of Temperature

Sun's radiations are composed of light and heat. Temperature has no effect on the amount of solar energy that reaches the PV panel. However, it reduces the amount of energy converted into electrical energy.

An increase in temperature will result in a reduction in the band gap energy; thereby will affect the semiconductors parameters. The decrease in the band gap of a semiconductor with increasing temperature is interpreted as increasing the energy of the electrons in the material; hence lower energy is needed to break the bond. Thus, less energy is required in order to take electrons from a lower energy state to a higher energy state.

In a solar cell , the parameter most affected by an increase in temperature is the open circuit voltage. The impact of increasing temperature on an I-V curve is shown in the figure below.

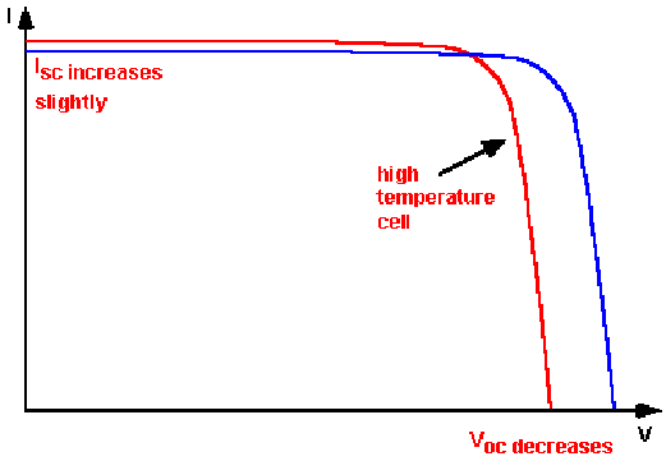

Figure2.6. Effect of temperature on the I-V characteristics [11]

2.7 Effect of Light Intensity

Photovoltaic cell parameters highly depend on the light intensity incident; hence a small variation in light intensity will change the short-circuit current, the open-circuit voltage , the fill factor , the efficiency and the impact of series and shunt resistances . The standard test light intensity is 1 kW/m² or AM 1.5.

Solar cells are subject to daily variations in light intensity . At low light levels , the effect of the shunt resistance becomes more important. When light intensity decreases, the current in the PV cell also decreases, and its equivalent resistance approaches the value of the shunt resistance. When these two are equal, the amount of the current flowing through the shunt resistance increases ; this, increases the fractional power loss due to the shunt resistance. Thus, in a cloudy day, a solar cell shunt resistance retains a greater fraction of its original power than a solar cell with a low shunt resistance.

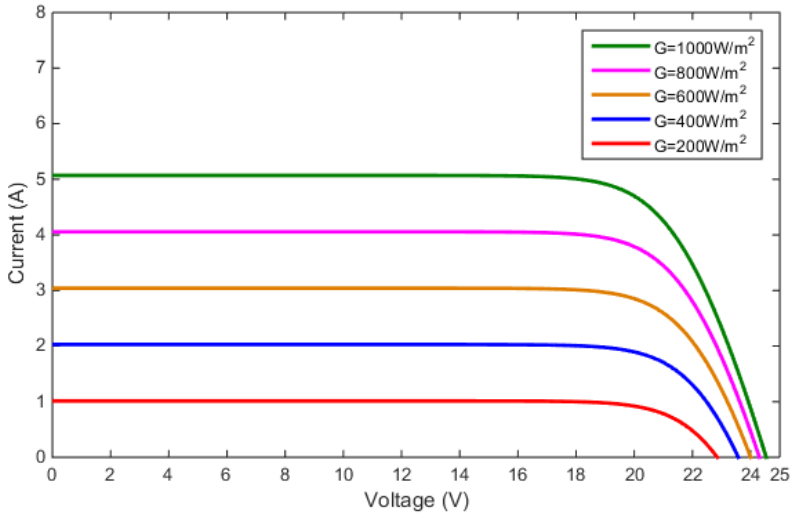

Figure2.7. Effect of light intensity on the I-V characteristics [12]

2.8 Advantages of Solar Energy

- Solar energy is a non-polluting, clean, reliable and renewable source of energy. It is environmentally friendly, transformed to electricity by means of solar panels that can reduce the dependence on fossil fuels. It is also considered to be an interesting prospect for countries that are aiming to go completely green in the next decades.

- Solar energy is used to produce electricity as long as the sun exists, it does not require any fuel, thus avoids problems related to fuel transportation and storage of radioactive waste.
- One of the most interesting things about solar installations is that they are energy independent, can be used at any building by installing PV panels. They are easy to install and do not require any wires, or power sources.
- The cost of installing the solar panels may be high. However, it is insignificant comparing to the benefits that a solar installation provide .First of all, it has a high reliability, as a result, it needs a minimal maintenance .Second, it is noise free and includes no moving parts .
- Solar installations are easily expanded.

CHAPTER THREE:

PV Modeling and Characterization

3.1 Introduction

To analyse characteristics of solar cells, electrical equivalent circuits are needed and hence modeled using simulation software. Researchers have developed mathematical models to understand and predict the effect of changing conditions on photovoltaic electrical output. Lumped parameter model is one of these models classified based on the number of diodes. This latter model is widely used and has proven to be more successful. The lumped parameter models are single diode model, double diode model and the three diode model. Although the accuracy of the characteristics of the model improves as the number of diode increases, the required mathematical expressions to obtain the output characteristics become more complex. For simplicity, in this project the single diode, known as the five parameter model, is the chosen model for the identification of photovoltaic cell parameters.

3.1.1 Real Single Diode Model

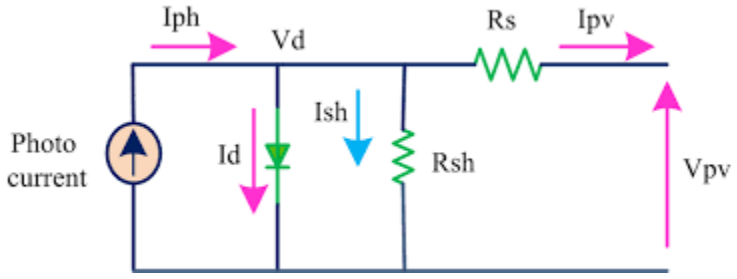

Figure3.1. Real single diode model for PV cell

The above model is an equivalent circuit of a practical single-diode photovoltaic cell. Based on the application of Kirchhoff's current law at any node in the circuit, the governing equation for this equivalent circuit is derived:

$$I = I_{ph} - I_d - I_{sh} \tag{3.1}$$

Where I_{ph} represents the light-generated current in the cell, I_d represents the voltage dependent current lost to recombination, and I_{sh} represents the current lost due to shunt resistance.

In this single diode model, I_d is modelled using the Shockley equation for an ideal diode:

$$I_d = I_s \left[e^{\left(\frac{V+I*R_s}{n*V_t}\right)} - 1 \right] \tag{3.2}$$

Where n is the diode ideality factor (unitless, usually between 1 and 2 for a single junction cell), I_s is the saturation current, and V_t is the thermal voltage given by:

$$V_t = \frac{K*T}{q} \tag{3.3}$$

Where, k is Boltzmann's constant ($K = 1.381 * 10^{-23} J/k$) and q is the elementary charge ($q = 1.602 * 10^{-19} C$).

By applying Kirchhoff's voltage law in the circuit, the shunt current can be written as,

$$I_{sh} = \frac{V+I*R_s}{R_{sh}} \tag{3.4}$$

Combining this equation with the above equations results in the complete governing equation for the single diode model:

$$I = I_{ph} - I_s \left[e^{\left(\frac{V+I*R_s}{n*V_t}\right)} - 1 \right] - \frac{V+I*R_s}{R_{sh}} \tag{3.5}$$

Then the five parameters of single diode model are:

- I_s: Diode saturation current (A).
- n: Diode ideality factor (1 < n < 2).
- R_s: Series resistance (Ω).
- R_{sh}: Shunt resistance (Ω).
- I_{ph}: Photocurrent (A).

Single-diode model takes into account different properties of solar cell as:

- R_s is introduced as to consider the voltage drops and internal losses due to flow of current. - R_{sh} takes into account the leakage current to the ground when diode is in reverse biased. But this model has neglected recombination effect of diode; therefore, it is still not the most accurate model.

3.2 Effect of Series and Parallel Resistances

i. Series resistance R_s

Series resistance does not affect the solar cell at open-circuit voltage since the overall current through the series resistance is zero. However, near the open-circuit voltage, the IV curve is strongly affected by the series resistance. A straight-forward method of estimating the series

resistance from a solar cell is to find the slope of the I-V curve at the open-circuit voltage point.

The main impact of series resistance is reducing the fill factor, although excessively high values of R_s may also reduce the short-circuit current.

Ignoring the parallel resistance and considering only series resistance; the equation of current reduces to the following:

$$I = I_{ph} - I_s \left[e^{\left(\frac{V+I*R_S}{n*V_t}\right)} \right] \tag{3.6}$$

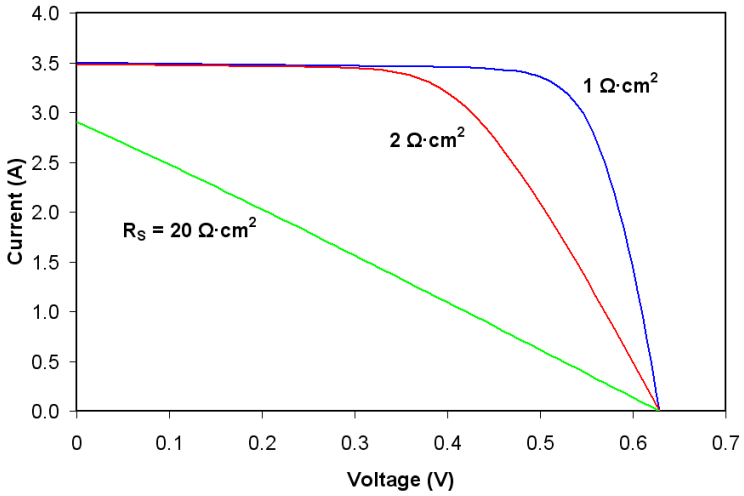

Figure3.2. Effect of series resistance on the I-V curve [13]

ii. Parallel Resistance R_{sh}

The presence of shunt resistance in photovoltaic cell causes significant power losses. These losses are due to manufacturing defects rather than poor solar cell design. Low shunt resistance causes power losses in solar cells by providing an alternate current path for the light-generated current. This diversion in the current path reduces the amount of current flowing through the solar cell junction and the voltage from the solar cell. The effect of a shunt resistance is particularly severe at low light levels, since there will be less light-generated current that will be lost to the shunt resistance .Moreover, at lower voltages where the effective resistance of the solar cell is high, the impact of a resistance in parallel is large.

The shunt resistance is found using the slope of the I-V curve at the short circuit current point. The equation of a solar cell with a shunt resistance only is as follows:

$$I = I_{ph} - I_s \left[e^{\left(\frac{V}{n*V_t}\right)} - 1 \right] - \frac{V}{R_{sh}} \tag{3.7}$$

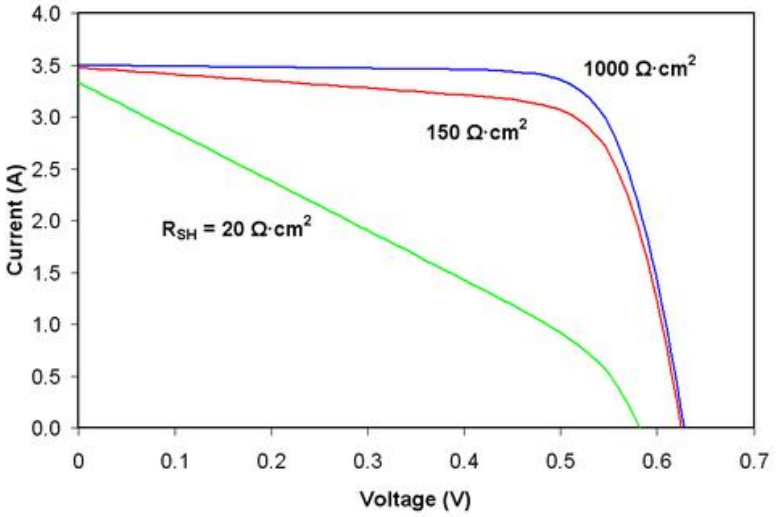

Figure3.3. Effect of shunt resistance on the I-V curve [13]

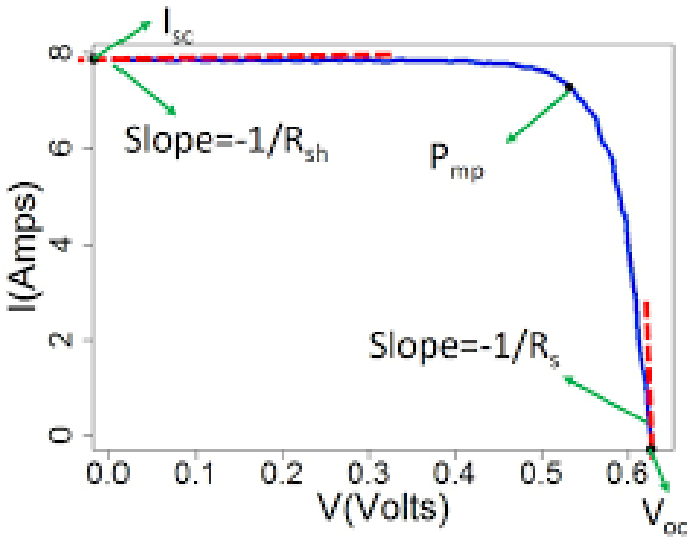

Figure3.4. Series and parallel resistances identification from I-V curve

3.3 Identification of PV Cell Parameters

3.3.1 Optimization algorithms

The current versus voltage relationship of the single diode PV cell model was presented in equation (3.5) and it was noticed that the equation of the I-V curve is nonlinear, which is difficult to solve by the analytical methods. Due to this difficulty scientists have developed several algorithms in order to solve this equation to determine the parameters of the solar cell. These algorithms are divided into two main categories:

i. Local Optimization Algorithms

Local optimization finds the optimal value within the neighboring set of candidate solutions. The performance of these methods, generally, strongly depends on the initial values supplied. This means that optimization might need to be run several times, with different initial guesses. Newton Raphson (NR) method is an example in this category. NR uses an initial guess to start with, and the n-iterations are performed until a local optimum is obtained. The drawback is if the initial guess is far from the actual solution this method will be stuck and diverge.

ii. Global Optimization Algorithms

The global optimization of a function or a set of functions is done according to some criteria. Typically, a set of bound and constraints .Those are considered in the optimization of the decision variables. It is distinguished from regular optimization by its focus on finding the maximum or minimum over all input values, as opposed to finding local minima or maxima [14].A global optimization algorithm does not need initial guess, and it provide more accurate results because of its ability to find and use the global optima of the cost function instead of the local optima.

For this project, metaheuristics are used. Metaheuristics can be adapted to solve a wide range of optimization problems. These methods are designed to find a good solution among a large set of feasible solutions with less computational effort than other optimization techniques.

3.3.2 ODM Parameters Extraction from Datasheet using GWO Estimation Method

i. Grey Wolf Optimization

Grey Wolf Optimization (GWO) is a population based meta-heuristic optimization method inspired by grey wolves (Canis lupus). The GWO algorithm mimics the leadership hierarchy and hunting mechanism of grey wolves in nature. The pack is classified into four groups, alpha, beta, delta, and omega for simulating the leadership hierarchy. Alpha is the first level and is the leader of the pack. Beta is the second level on the hierarchy of wolves, they help alpha wolves to make a decision .Delta represent the third level in the pack, delta wolves have to succumb to alpha and beta, however, they dominate omega. Omega wolves have the lowest position in the pack; they have to succumb to all other dominant wolves. Figure 3.5 shows the grey wolf social hierarchy [15].

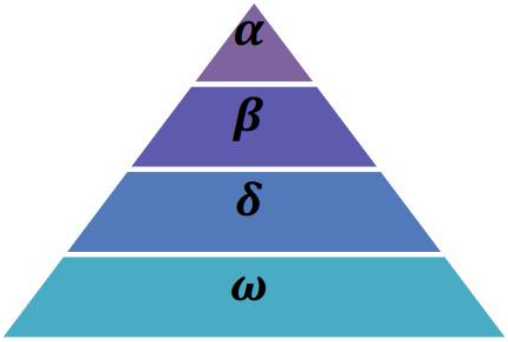

Figure3.5. Hierarchy of grey wolf

In addition to the social hierarchy of wolves, group hunting is another interesting social behavior of grey wolves. According to Muro et al. [16] the main phases of grey wolf hunting are as follows:

- Tracking, chasing and approaching the prey.
- Following, encircling, and harassing the prey until it stops moving.
- Attacking the target.

Figure3.6. Hunting conduct of grey wolves: (A) approaching and pursuing target, (B-D) following, encircling and disturb the target, (E) attacking the target. [16]

Wolves encircle the target during the chase. The encircling is modeled by the equations (3.8) and (3.9) [16]:

$$\vec{D} = |\vec{C}.\overrightarrow{X_p}(t) - \vec{X}(t)| \quad (3.8)$$

$$\vec{X}(t+1) = \overrightarrow{X_p}(t) - \vec{A}.\vec{D} \quad (3.9)$$

Where t represents the current iteration, $\vec{A}$, $\vec{C}$ and $\overrightarrow{D}$ are coefficient vectors, $\overrightarrow{X_p}$ is the position vector of the victim, and $\vec{X}$ is the position vector of a grey wolf

$\vec{A}$ and $\vec{C}$ are computed through these two equations:

$$\vec{A}= 2\,\vec{a}\,.\,\overrightarrow{r_1} - \vec{a} \tag{3.10}$$

$$\vec{C}= 2\,\overrightarrow{r_2} \tag{3.11}$$

Components of $\vec{a}$ linearly reduces from 2 to 0 through the iterations and $\overrightarrow{r_1}$ and $\overrightarrow{r_2}$ are random vectors in [0, 1].

The pursuit is habitually directed by the leader alpha (α) followed by beta (β) and delta (δ) which can sometimes contribute in chasing. (δ) and (ω) look after the injured wolves in the group. Alpha (α) is considered the best result attributed to it the best information of the place of the target , beta (β) and delta (δ) are the second and the third best solutions respectively in designing GWO. Omega is the last best. Therefore, the first three best solutions obtained so far, are saved and the other search agents (including the omegas) are obliged to update their positions according to the position of the best search agent .When the prey stops moving, the wolves terminates the chase by attacking it.

In this regard, the following formulas are applied:

$$\begin{cases} \overrightarrow{D_\alpha}= |\overrightarrow{C_1}.\overrightarrow{X_\alpha}(t) - \vec{X}(t)| \\ \vec{X}_1= \overrightarrow{X_\alpha}(t) - \overrightarrow{A_1}.\overrightarrow{D_\alpha} \end{cases} \tag{3.12}$$

$$\begin{cases} \overrightarrow{D_\beta}= |\overrightarrow{C_2}.\overrightarrow{X_\beta}(t) - \vec{X}(t)| \\ \vec{X}_2= \overrightarrow{X_\beta}(t) - \overrightarrow{A_2}.\overrightarrow{D_\beta} \end{cases} \tag{3.13}$$

$$\begin{cases} \overrightarrow{D_\delta}= |\overrightarrow{C_3}.\overrightarrow{X_\delta}(t) - \vec{X}(t)| \\ \vec{X}_3= \overrightarrow{X_\delta}(t) - \overrightarrow{A_3}.\overrightarrow{D_\delta} \end{cases} \tag{3.14}$$

$$\vec{X}(t+1)= \frac{\vec{X}_1+\vec{X}_2+\vec{X}_3}{3} \tag{3.15}$$

ii. GWO Estimation Method

The proposed five-parameter estimation method is based on the three points that characterize the I-V curve, which are the maximum power point (V_{mpp} , I_{mpp}) , short circuit point (0, I_{sc}) and open circuit point (V_{oc} , 0). It regards the optimization of the ideality factor n, the parallel resistance R_{sh} , the saturation current I_s , the series resistance R_s , and the photo current I_{ph} using the data provided in the datasheet.

Like any optimization algorithm, an objective function F(X) should first be set. F(X) is based on the single diode equation (equation (3.5)). For the identification of PV module parameters, the number of series connected cells N_s is considered, and the equation becomes:

$$I = I_{ph} - I_s \left[e^{\left(\frac{V+I*R_s}{n*N_s*V_t}\right)} - 1 \right] - \frac{V+I*R_s}{R_{sh}} \tag{3.16}$$

Thus, the objective function is:

$$\begin{cases} F(X) = I - I_{ph} + I_s \left[e^{\left(\frac{V+I*R_s}{n*N_s*V_t}\right)} - 1 \right] + \frac{V+I*R_s}{R_{sh}} \\ X = \{I_{ph}, I_s, R_s, n, R_{sh}\} \end{cases} \tag{3.17}$$

The fitness function that needs to be minimized by this algorithm, in order to quantify the error is the root mean square error RMSE between the approximated values in the datasheet I_{mpp} , I_{sc} , I=0 at open circuit condition and the calculated ones.

$$\text{Fitness} = \text{RMSE} = \sqrt{\frac{1}{3}\sum_1^3 (I_{Datasheet} - I_{calculated})^2} \tag{3.18}$$

Then, the NRMSE error is calculated as follows:

$$\text{NRMSE} = \frac{\text{RMSE}}{\sqrt{\frac{1}{3}*\sum_1^3 I_{Datasheet}{}^2}} * 100 \tag{3.19}$$

The pseudo code of the proposed algorithm is presented in Figure 3.7 and its flowchart is shown in Figure3.8.

Algorithm 1: The main procedure of GWO

Input: T, N_s , V_{mpp} , I_{mpp} , V_{oc} , I_{sc}

Output: X_α

Initialize the grey wolf population Xi (i=1, 2, ... n)

Initialize a, A, and C

Calculate the fitness of each search agent by Eq.(3.18)

X_α= the best search agent

X_β = the second best search agent

X_δ = the third best search agent

while (t < Max number of iterations)

for each search agent

Update the position of the current search agent by equation (3.15)

end for

Update a ,A ,and C

Calculate the fitness of all search agents by Eq.(3.18)

Update X_α , X_β ,and X_δ

t=t+1

end while

return X_α

Calculate NRMSE using equation (3.19)

end procedure

Figure3.7. The pseudo code of the proposed algorithm.

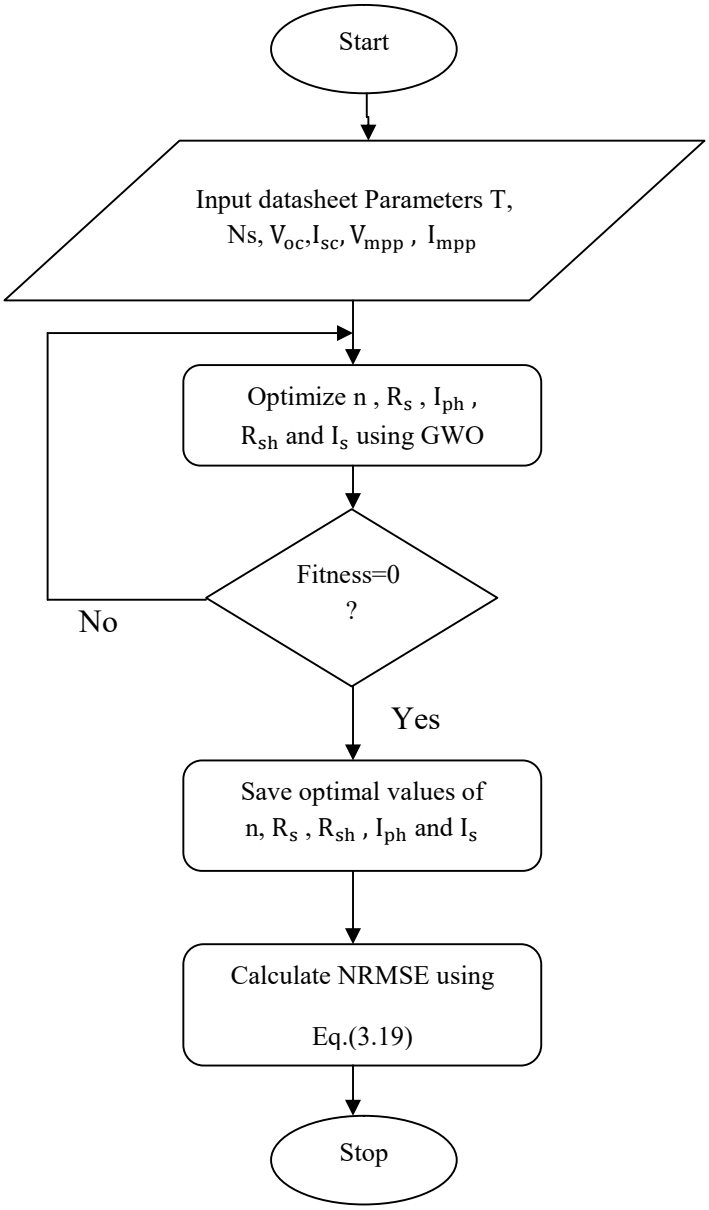

Figure3.8. The proposed five parameters estimation method

3.3.3 PV Module P-V and I-V Characteristics Using SIMULINK

i. MATLAB:

MATLAB is a mathematical and graphical software package with numerical, graphical, and programming capabilities. The name MATLAB stands for matrix laboratory. MATLAB has built-in functions to perform many operations, and there are toolboxes that can be added to augment these functions. There are versions available for different hardware platforms, in both professional and student editions.[17] Its typical uses include:

- Math and computation

- Algorithm development
- Modeling, simulation, and prototyping
- Data analysis, exploration, and visualization
- Scientific and engineering graphics
- Application development, including Graphical User Interface building

Toolboxes allow the user to learn and apply specialized technology. They are comprehensive collections of MATLAB functions (M-files) that extend the MATLAB environment to solve particular classes of problems. Areas in which toolboxes are available include signal processing, control systems, neural networks, fuzzy logic, wavelets, simulation, and many others [18].

ii. SIMULINK:

SIMULINK is a MATLAB-based graphical programming environment for modeling, simulating and analyzing multi-domain dynamical systems. Its primary interface is a graphical block diagramming tool and a customizable set of block libraries. It offers tight integration with the rest of the MATLAB environment and can either drive MATLAB or be scripted from it. SIMULINK is widely used in automatic control and digital signal processing for multi-domain simulation and model-based design [19].

iii. PV Module an ODM _GWO based Simulation

The photovoltaic ODM_GWO simulation is modeled based on the equation (3.16) and the proposed GWO algorithm.

Mainly, the parameters extraction is conducted for the electrical performance under standard test conditions STC (T_{STC} = 298.15 K° and $G_{STC} = 1000\ W/m^2$) using the electrical specifications provided in the datasheet. The simulation is enhanced to provide I-V and P-V characteristics under varying environmental conditions, using the following equations [20]:

$$I_{ph}(T,G) = \left[I_{ph\,STC} + K_i * (T - T_{STC})\right] * \frac{G}{G_{STC}} \quad (3.20)$$

$$n(T,G) = n_{STC} * \frac{T_{STC}}{T} \quad (3.21)$$

$$I_s(T,G) = \frac{I_{ph\,STC} + K_i * (T - T_{STC})}{e^{\frac{V_{oc} + K_V * (T - T_{STC})}{n(T,G) * N_S * V_t(T,G)}} - 1} \quad (3.22)$$

$$R_s(T,G) = R_{s\,STC} * \frac{T}{T_{STC}}\left(1 - 0.217 \ln\left(\frac{G}{G_{STC}}\right)\right) \quad (3.23)$$

$$R_{sh}(T,G) = R_{sh\,STC} * \frac{G_{STC}}{G} \quad (3.24)$$

Where, K_i is the temperature coefficient of the short circuit current and K_v is the temperature coefficient of the open circuit voltage.

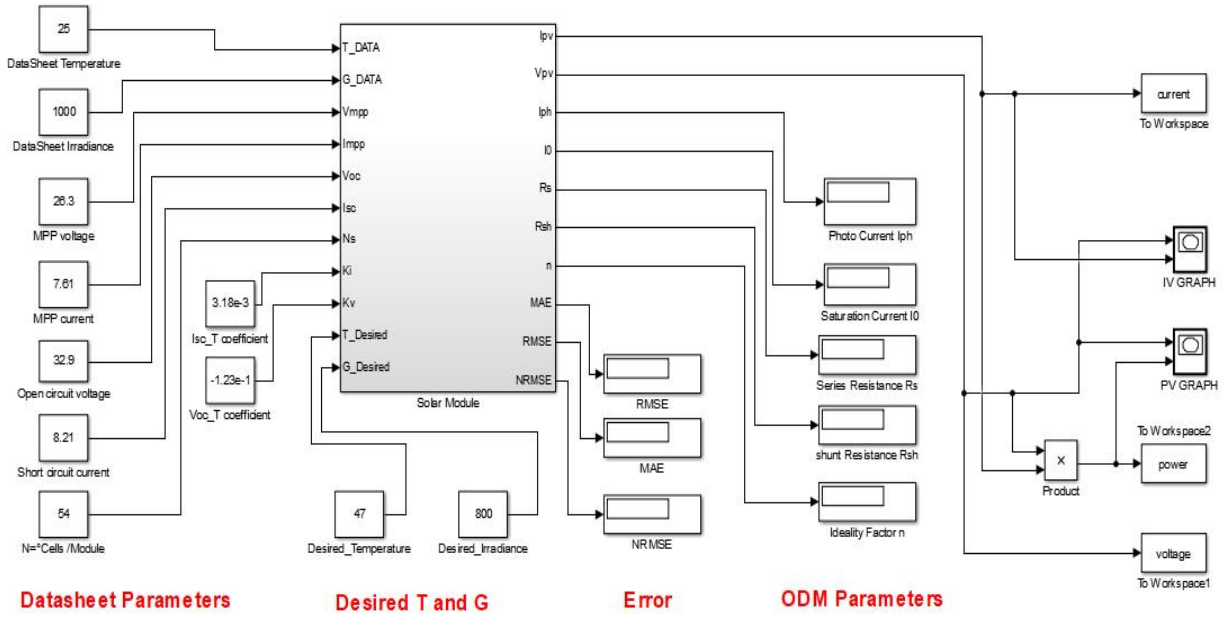

Figure3.9. PV Module I-V and P-V Characteristics based on ODM Simulation

3.3.4 PV Module Parameters Identification from Measured I-V Data

i. Particle Swarm Optimization

Particle Swarm Optimization (PSO) is a population based metaheuristic global optimization technique inspired by the motion of bird flocks and schooling fish. PSO algorithm searches the space of an objective function by adjusting the trajectories of individual agents, called particles. A population of these particles flies through the search space such that each particle i is attracted toward the position of the current global best g* and its own best location x^i in history, while at the same time it has a tendency to move randomly. Initially, the particles are randomly placed in the search space. The objective function is evaluated for all the particles; When a particle i finds a location that is better than any previously found locations, it updates it as the new current best x^i by updating velocity first depending on movement inertia, self-cognition, and social interaction using equation (3.25) then updating its position through equation (3.26) at each iteration .Thus, There is a current best for all n particles at any time t

during iterations. The aim is to find the global best among all the current best solutions until the objective no longer improves or after a certain number of iterations. The movement of particles is schematically represented in Figure 3.10 where x* is the current best for particle i , and g* ={(x^i)} for (i=1,2, ...n) is the current global best.[21]

$$v_{n+1}^i = w\, v_n^i + c_1 r_1 \left[p_n^i - x_n^i\right] + c_2 r_2 \left[p_n^g - x_n^i\right] \quad (3.25)$$

$$x_{n+1}^i = x_n^i + v_{n+1}^i \quad (3.26)$$

Where:

x^i is the position of the i^{th} particle in the search space.

v^i is the velocity of the i^{th} particle

w is particle inertia

c_1 is cognitive acceleration constant

c_2 is social acceleration constant

p^i is particle's best known position

p^g is the best known swarm position found by all particles (global best position)

r_1 , r_2 are random numbers between 0 and 1

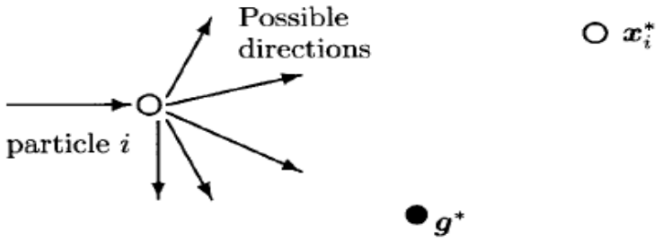

Figure3.10. Schematic representation of the motion of a particle in PSO

ii. Opposition Based Initialization

In PSO, the starting points are given randomly. If the starting points are close to the optimal point, convergence speed would be faster .Thus, a better and careful initialization based on priori information can lead to better results. The proposed method for an improved PSO algorithm is an opposition based initialization of the swarm. This approach consists of initializing the PSO population and its opposite population. The fitness function is evaluated

for both populations and only the fitter particles are selected to form a new population for the PSO. The concept used is described below.

- Particle: a swarm particle p^i is defined as:

$p^i \in [a, b]$ such that, i=1,2,…, D and a, b ϵ R

D represents dimensions, and R represents real numbers

- Opposite particle; every particle p^i has a unique opposite p^i_{op} defined as:

$$p^i_{op} = a + b - p^i \text{ such that, } i=1, 2,\dots D \text{ and } a, b \in R \quad (3.27)$$

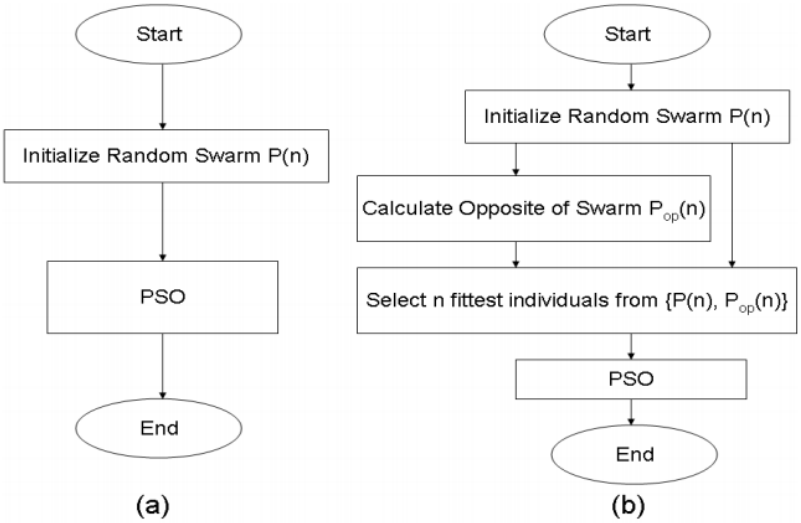

Figure3.11. PSO with (a) Random population initialization and (b) Opposition based population initialization

iii. ODM Parameters Extraction using an IOB-PSO

The following objective function is used,

$$\begin{cases} F(X) = I - I_{ph} + I_s \left[e^{\left(\frac{V+I*R_s}{n*N_s*V_t}\right)} - 1 \right] + \frac{V+I*R_s}{R_{sh}} \\ X = \{I_{ph}, I_s, R_s, n, R_{sh}\} \end{cases} \quad (3.28)$$

The fitness function that needs to be minimized by this algorithm, in order to quantify the error between the measured and calculated data is the root mean square error (RMSE),

$$\text{Fitness} = \sqrt{\frac{1}{N}\sum_1^N F(X)^2} \quad (3.29)$$

The pseudo code of the PSO algorithm is presented In Figure 3.12 and its corresponding flowchart is shown in Figure 3.13.

Algorithm2: The main procedure of IOB-PSO

Input: T, Ns , V_{Data} , I_{Data}
Output: global best
for each particle
Initialize particle position
Initialize particle velocity
Calculate cost value of particles using equation (3.29)
Initialize opposite particle position using equation (3.27)
Initialize opposite particle velocity
Calculate cost value of opposite particles using equation (3.29)
If opposite particle cost < particle cost
Update particle
end if
Update particle best
If particle best cost < global best cost
Update global best
end if
end for
for (t =1: Max number of iterations)
for each particle
Update velocity using equation (3.25)
Update position using equation (3.26)
Calculate cost value using equation (3.29)
If particle cost < particle best cost
Update particle best
If particle best cost < global best cost
Update global best
end if
end if
end for
end for
return global best
end procedure

Figure 3.12. The pseudo code of the IOB-PSO algorithm.

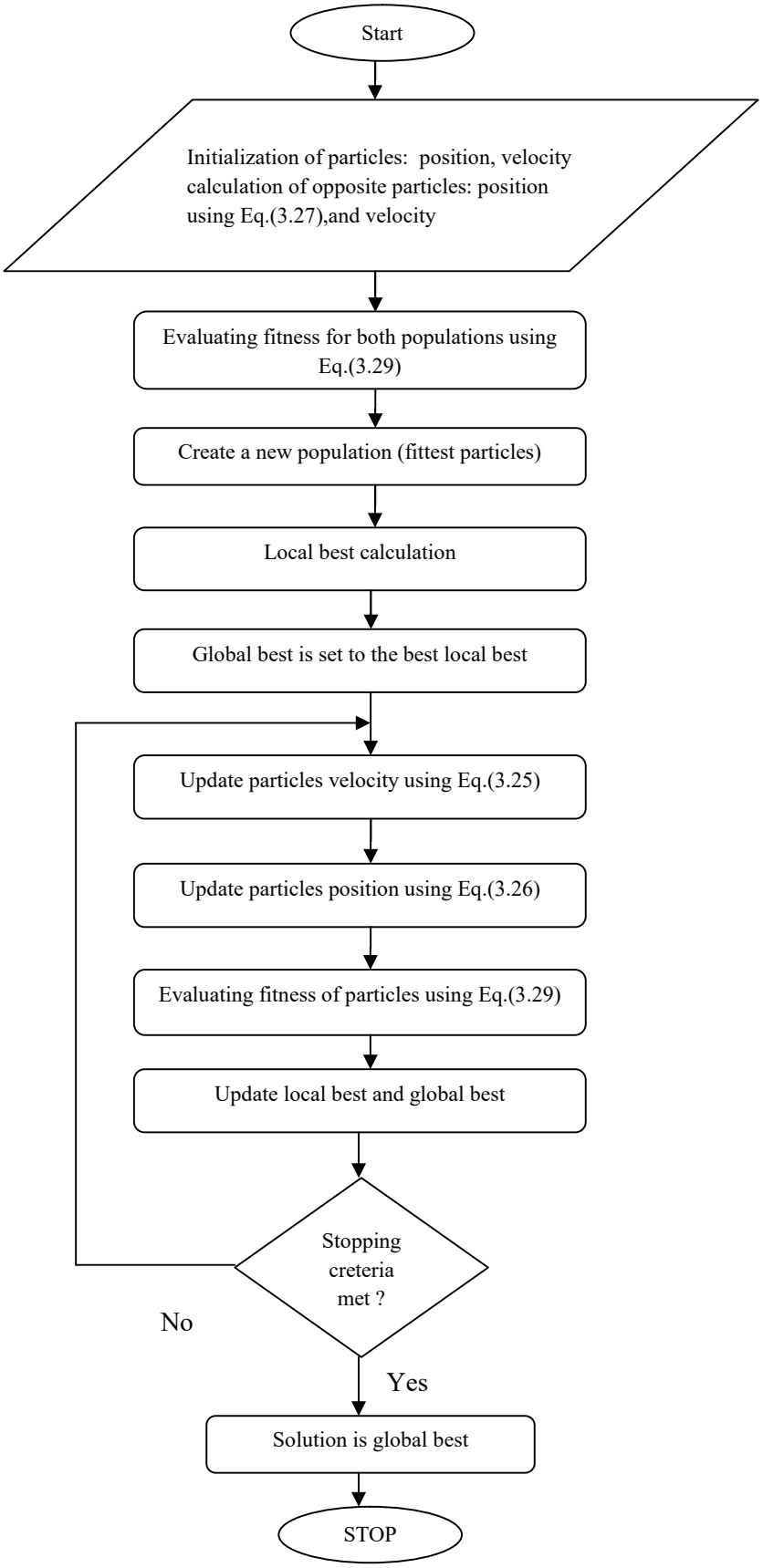

Figure3.13. Flowchart of improved opposition based Particle swarm optimization

CHAPTER FOUR:

Results and Discussion

Chapter 4

Simulation Results

4.1 GWO based ODM Simulation

In this section, the GWO based ODM simulator is tested for four different PV modules. The PV simulator is implemented in MATLAB R2016a and executed on a PC with Intel® Core™ i5-2450M CPU processor @ 2.50GHz, 4GB RAM , under Windows 10 64-bit OS. The search ranges used in the optimization of the five parameters are:

Table4.1.ODM parameter search ranges

Parameter	Search range
I_{ph}	$[0.95 \times I_{sc}\ , 1.05 \times I_{sc}\ ]$
I_s	[1μA, 5 μA]
n	[1, 2]
R_{sh}	$[\frac{V_{mpp}}{I_{sc}-I_{mpp}}\ , 1500\ \Omega\ ]$
R_s	$[0\ , \frac{V_{mpp}-V_{oc}}{I_{mpp}}\ ]$

The GWO parameters are presented in Table 4.2.

Table 4.2.GWO parameters

Parameters	Value
Random values r1, r2	[0, 1]
No. of search agents	30
Maximum iteration	1000

The datasheets parameters of used PV modules are presented in Table 4.3.

Table4.3.Datasheet Parameters

Module	Type	V_{mpp}[V]	I_{mpp}[V]	V_{oc}[V]	I_{sc}[V]	N_s	STC (T/G)
KC200GT	Poly-crystalline	26.3	7.61	32.9	8.21	54	25°c/1000w/m^2
BP MSX 120	Poly-crystalline	33.7	3.56	42.1	3.87	72	25°c/1000w/m^2
STM6-40/36	Mono-crystalline	18	2.23	21.6	2.36	36	25°c/1000w/m^2
QSMART 95	Thin-film	62.1	1.53	78	1.68	119	25°c/1000w/m^2

Case Study #1: KC200GT

The polycrystalline module KC200GT ODM parameters are extracted to draw the I-V and P-V characteristics using the developed PV simulator. The results obtained at STC are presented in Table 4.4. The GWO results for the KC200GT module are compared with other published methods results to prove its efficiency.

Table4.4. KC200GT parameters at STC achieved by different methods.

Methods	Parameters					Error	
	$I_{ph}[A]$	$I_s[\mu A]$	n	$R_s[\Omega]$	$R_{sh}[\Omega]$	RMSE[A]	NRMSE [%]
Villalva [22]	8.193	0.08520	1.300	0.13870	466.0	2.3e-1	3.02
Accarino [22]	8.193	0.00200	1.079	0.23630	204.0	1.1e-1	1.49
Stornelli [22]	8.220	0.00514	1.120	0.26560	144.9	1.2e-1	1.53
GWO*	8.212	1.06700	1.497	0.08988	201.4	1.305e-4	2.072e-2

* Proposed method

As given in Table 4.4, the normalized mean absolute error NRMSE obtained by the proposed method (0.02072 %) is the least which proves the effectiveness of this technique in extracting the unknown PV parameters. Moreover, the convergence using this method is very fast, where the simulation execution time is less than 7 s.

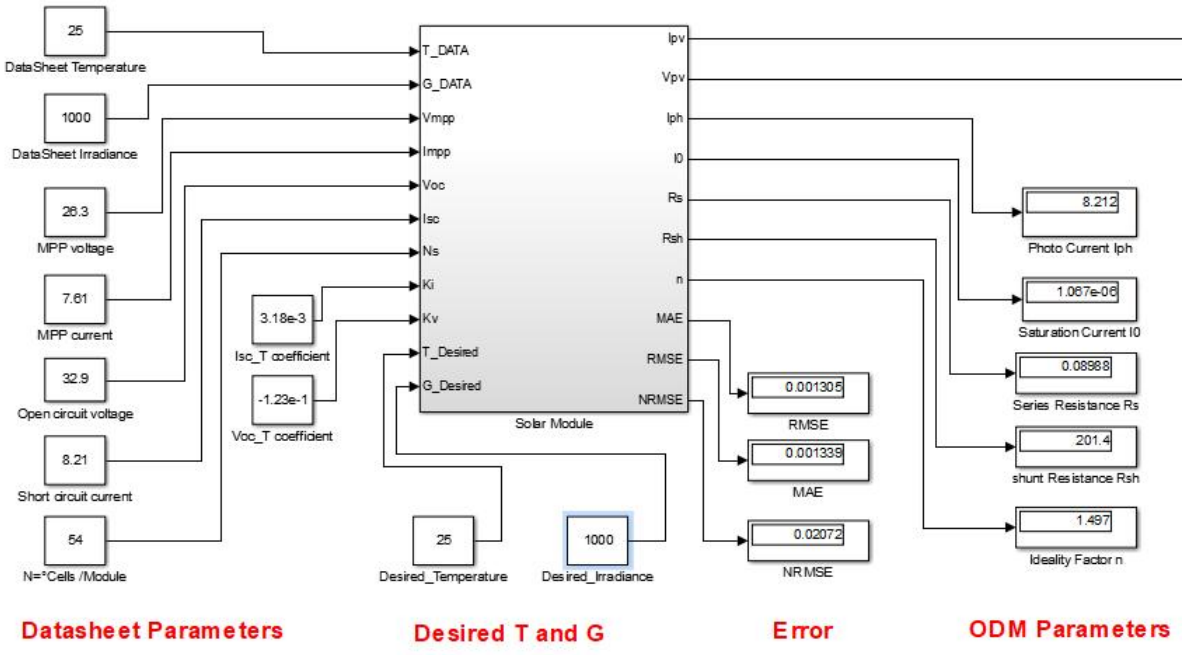

Figure4.1.KC200GT simulation results at STC

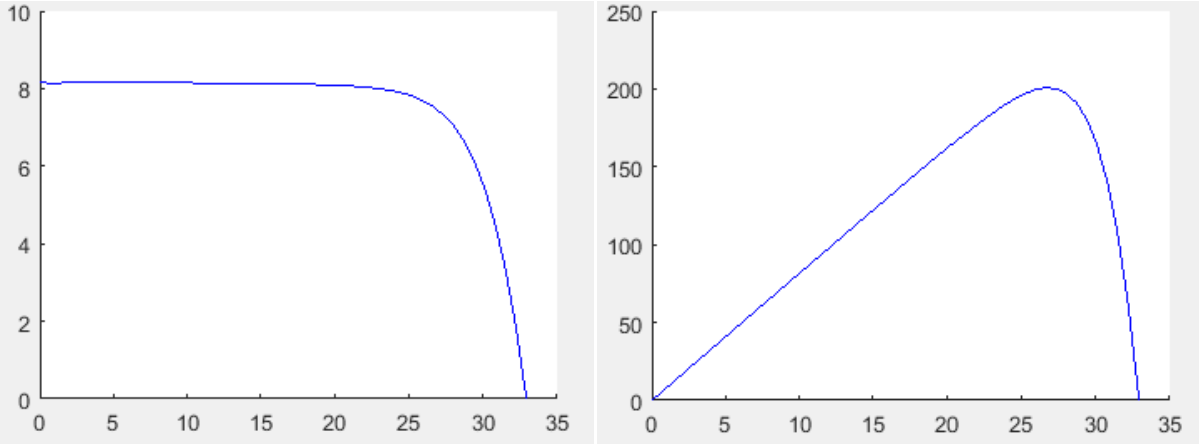

(a) (b)

Figure4.2. (a) I-V and (b) P-V characteristics of KC200GT at STC

Table4.5. Comparison of datasheet values and simulation model values at STC

(T/G)	Parameters	Datasheet Parameters	Parameters from the simulation of the model	Relative error (%)
STC	$V_{oc}[V]$	32.9	33.00	0.303951368
	$I_{sc}[A]$	8.21	8.148	0.755176614
	$V_{mpp}[V]$	26.3	26.60	1.140684410
	$I_{mpp}[A]$	7.61	7.5448	0.856774110
	$P_{max}[W]$	200	200.6906	0.345300000

The PV simulator is tested again for the KC200GT at the NOCT (T=47 °c and G=800w/m^2), the results are presented in Table 4.6 and Figure 4.3.The I-V and P-V characteristics obtained at NOCT are compared to The STC previously obtained curves as shown in Figure 4.4.

Table4.6. KC200GT parameters at STC and NOCT

(T/G)	Parameters				
	$I_{ph}[A]$	$I_s[\mu A]$	n	$R_s[\Omega]$	$R_{sh}[\Omega]$
STC	8.212	1.067	1.497	0.08988	201.4
NOCT	6.626	4.037	1.394	0.1012	251.7

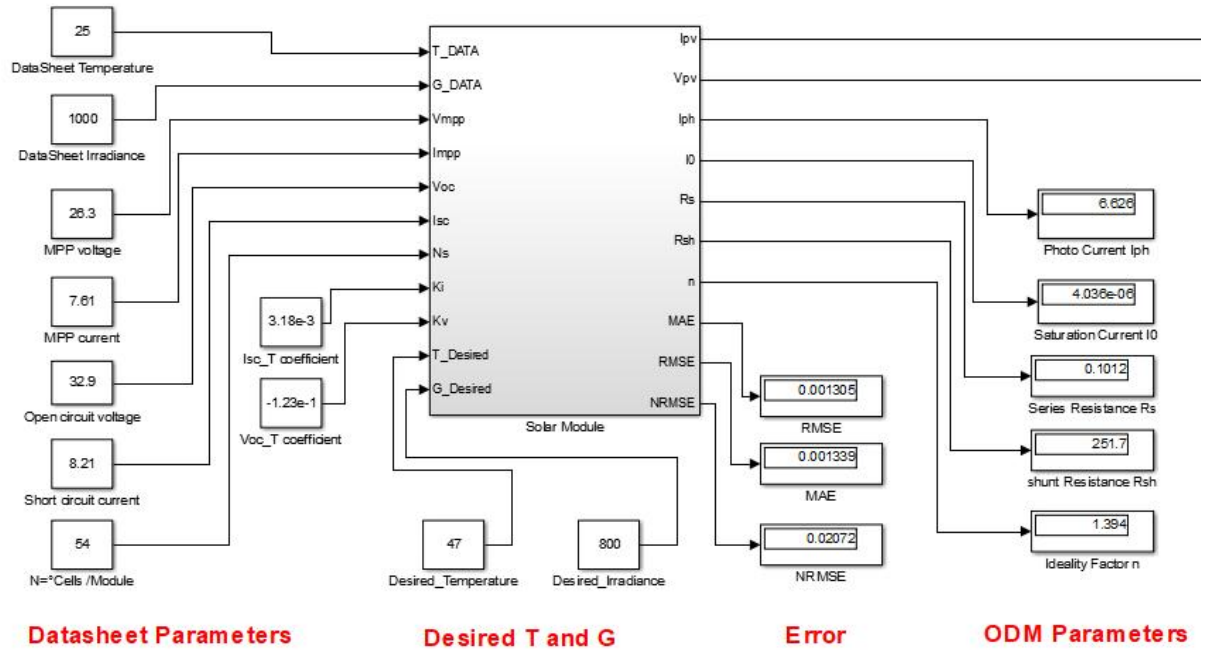

Figure4.3.KC200GT simulation results at NOCT

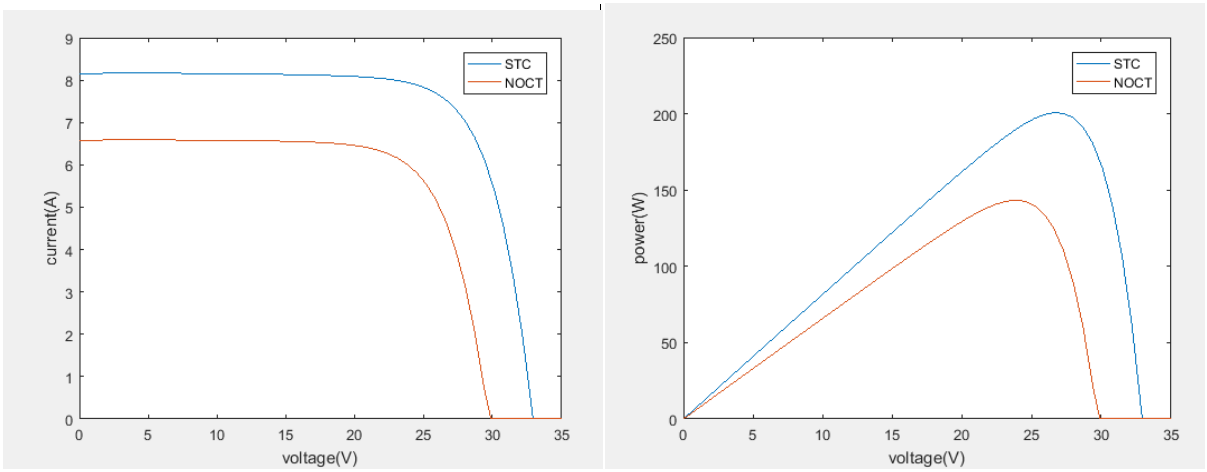

(a) (b)

Figure4.4. (a) I-V and (b) P-V characteristics of KC200GT

Table4.7. Comparison of datasheet values and simulation model values at NOCT

(T/G)	Parameters	Datasheet Parameters	Parameters from the simulation of the model	Relative error (%)
NOCT	V_{oc}[V]	29.9	29.9	0
	I_{sc}[A]	6.62	6.5745	0.687311178
	V_{mpp}[V]	23.2	23.80	2.586206900

I_{mpp}[A]	6.13	6.0229	1.747145190
P_{max}[W]	142	143.3442	0.946619718

Furthermore, in order to demonstrate the effect of irradiance on I-V and P-V curves, the simulation was executed at a constant temperature T=25°c and variable irradiance value .The obtained results for the extracted parameters are tabulated in Table4.8, and the resulted I-V and P-V characteristics are presented in Figure 4.5 .

Table4.8. KC200GT parameters at T=25°c and variant irradiance

T [°c]	G [w/m^2]	Parameters				
		I_{ph}[A]	I_s[μA]	n	R_s[Ω]	R_{sh}[Ω]
25	200	1.642	1.067	1.497	0.1213	1007.0
25	400	3.285	1.067	1.497	0.1078	503.5
25	600	4.927	1.067	1.497	0.09984	335.7
25	800	6.57	1.067	1.497	0.09423	251.7
25	1000	8.212	1.067	1.497	0.08988	201.4

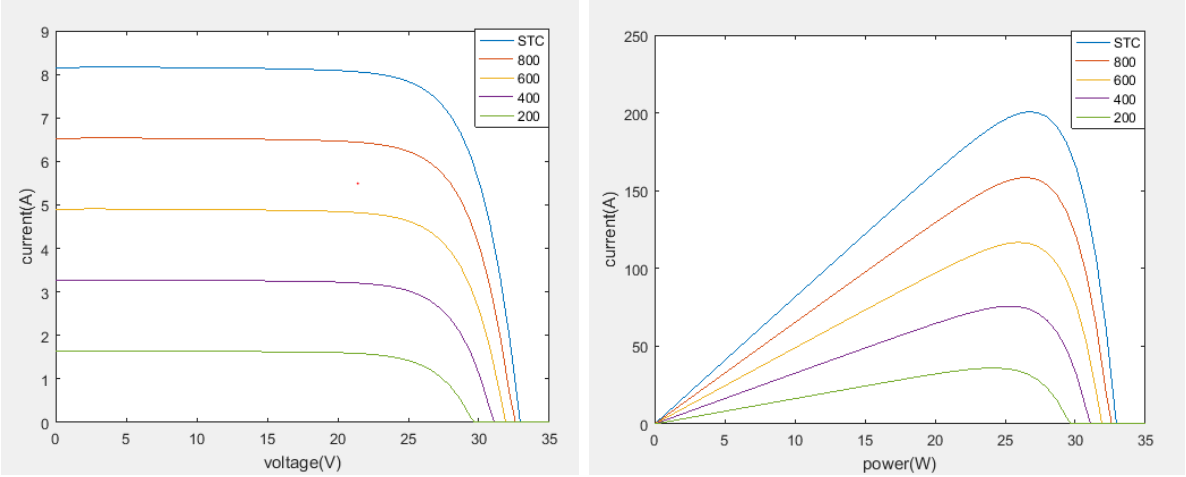

(a) (b)

Figure4.5. (a) I-V and (b) P-V characteristics of KC200GT at T=25°c and variant G

It is observed that the current increases while rising the irradiance intensity. This demonstrates that the irradiance has a substantial effect on short circuit current. However, the open circuit voltage increases slightly as shown in Figure4.5.Furthermore; it is deduced from

Figure 4.5.(b) that the power generation by PV model increases by increasing the intensity of solar irradiance.

Moreover, to demonstrate the effect of temperature on the I-V and P-V characteristics, the simulation was conducted at a constant irradiance G=1000 w/$m^2$and variable temperature value. The extracted parameters are tabulated in Table 4.9, and the resulted I-V and P-V characteristics are presented in Figure 4.6.

Table4.9. KC200GT parameters at G=1000 w/$m^2$and variable temperature

T [°c]	G [w/m^2]	Parameters				
		I_{ph}[A]	I_s[μA]	n	R_s[Ω]	R_{sh}[Ω]
25	1000	8.212	1.067	1.497	0.08988	201.4
50	1000	8.292	4.827	1.381	0.09742	201.4
75	1000	8.371	21.41	1.282	0.1050	201.4

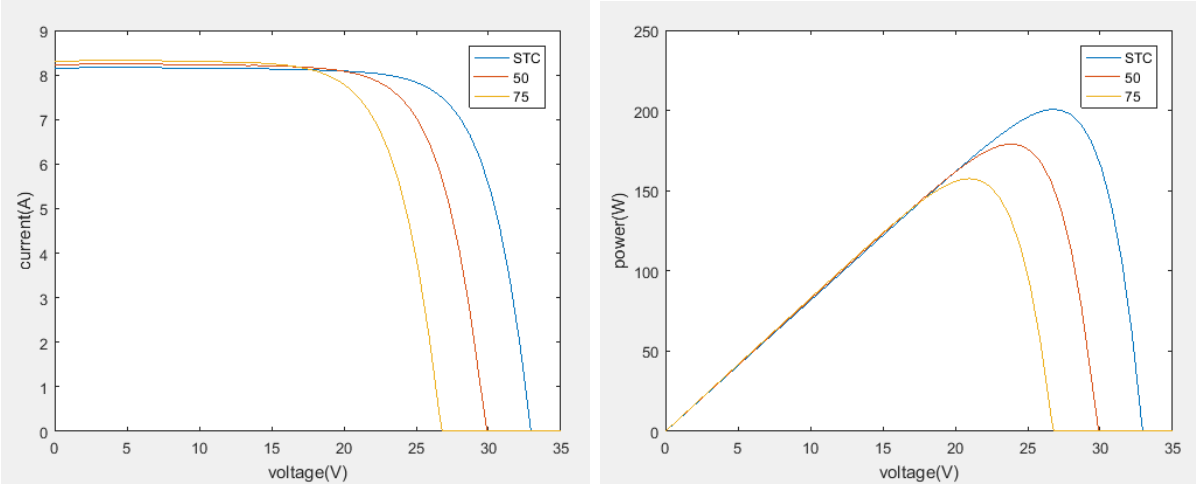

(a) (b)

Figure4.6. (a) I-V and (b) P-V characteristics of KC200GT at G=1000 w/$m^2$and variant T

The temperature demonstrates a significant effect on the output performance curves of PV solar module when irradiance intensity is kept constant at 1000 w/m^2.In current parameters, a minor variation is observed when temperature varies from 25°c to 75°c.The voltage shows increasing trend in I-V performance curve when the temperature reduces as illustrated in Figure4.6.(a). Also, the solar cell generates more power, when the atmospheric

temperature reduces as described in Figure4.6.(b).Thus solar cell shows inverse relationship with temperature.

The simulated I-V characteristics at different irradiances and temperatures are compared with the curves given by the manufacturer in the datasheet as shown in Figure 4.7.

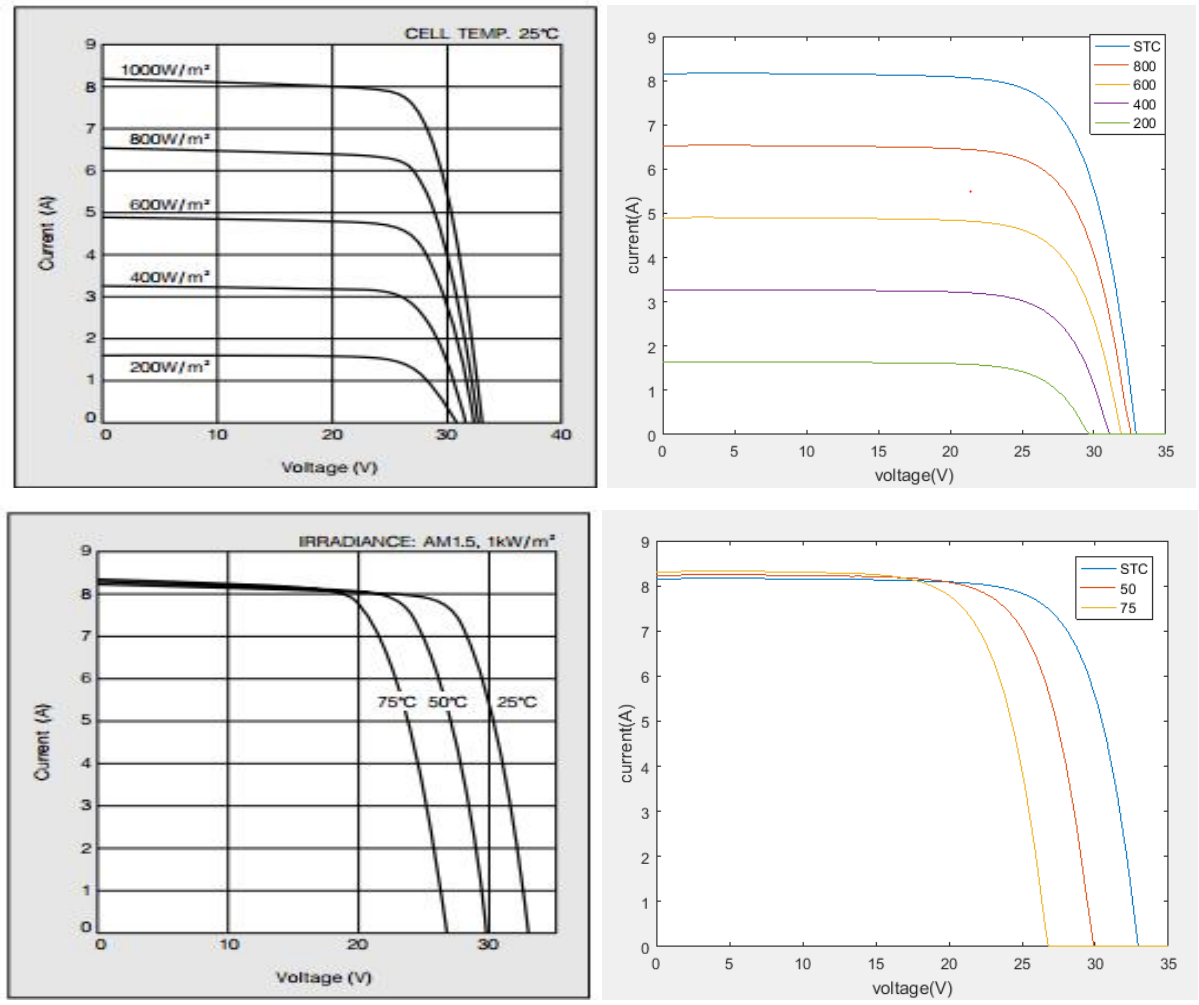

(a) (b)

Figure4.7. I-V characteristics of KC200GT (a) datasheet (b) Simulated

The comparison between simulated I-V curves and manufacturer provided characteristics shows that they are almost identical .Thus, the effectiveness of the proposed PV module simulator at different environmental conditions is proved.

Case Study #2: BP MSX 120

The multi-crystalline BP MSX 120 PV module's I-V and P-V characteristics are constructed using the simulation at STC and at T=40°c and G = 300 w/m^2 .The simulation results are

given in Table 4.10 and Figures 4.8 , 4.9 , 4.10 .The computed errors are: RMSE= 1.161e-3 and NRMSE= 4.399e-2 .

Table4.10. BP MSX 120 extracted parameters

T [°c]	G [w/m^2]	Parameters				
		I_{ph}[A]	I_s[μA]	n	R_s[Ω]	R_{sh}[Ω]
25	1000	3.870	1.884	1.567	0.1674	691.5
40	300	1.164	1.957	1.492	0.2218	2305.0

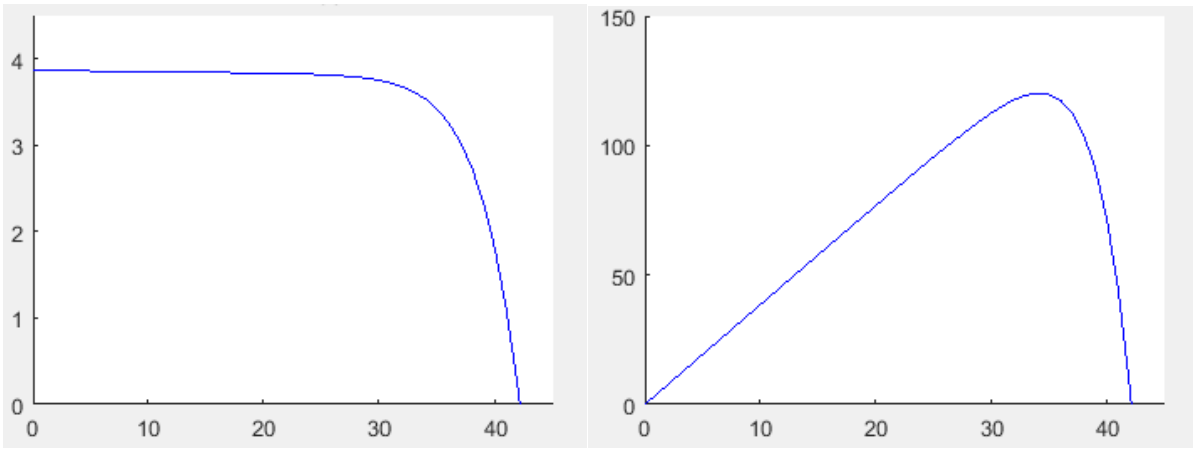

(a) (b)

Figure4.8. (a) I-V and (b) P-V characteristics of BP MSX 120 at STC

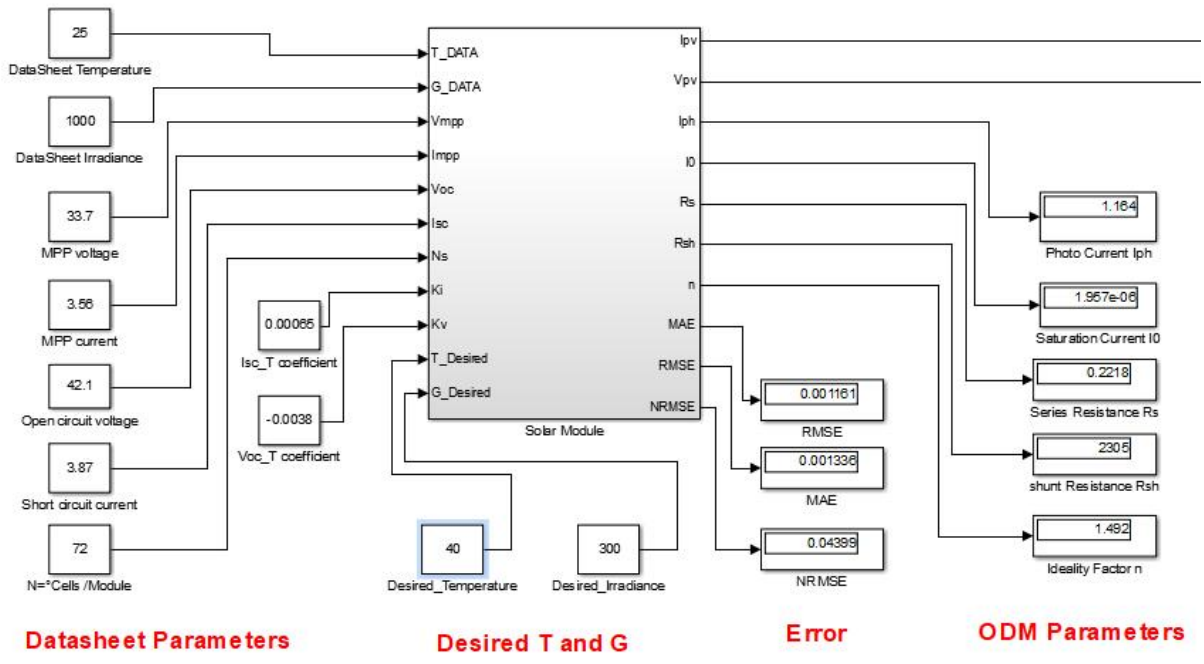

Figure4.9. BP MSX 120 simulation results at T=40°c and G = 300 w/m^2

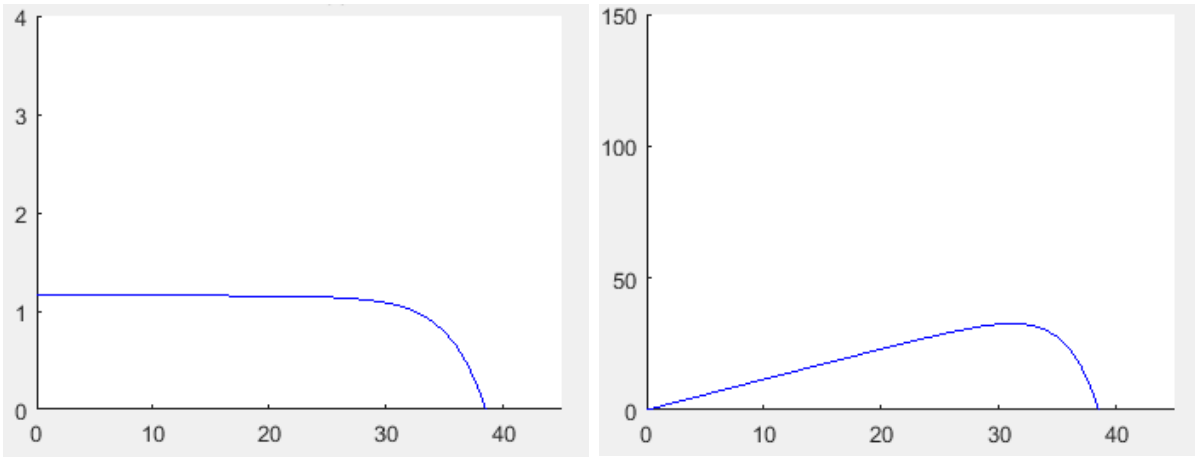

(a) (b)

Figure4.10. (a) I-V and (b) P-V characteristics of BP MSX 120 at T=40°c and G = 300 w/m^2

Case Study #3: STM6-40/36

The mono-crystalline module STM6-40/36 simulation results are extracted from datasheet parameters at STC as shown in Table 4.11 and Figure 4.11.

Table4.11. STM6-40/36 parameters at STC

T (°c)	Parameters					Error	
	I_{ph}[A]	I_s[μA]	n	R_s[Ω]	R_{sh}[Ω]	RMSE[A]	NRMSE [%]
STC	2.377	0.1506	1.409	0.01475	1490	1.19e-2	0.7671

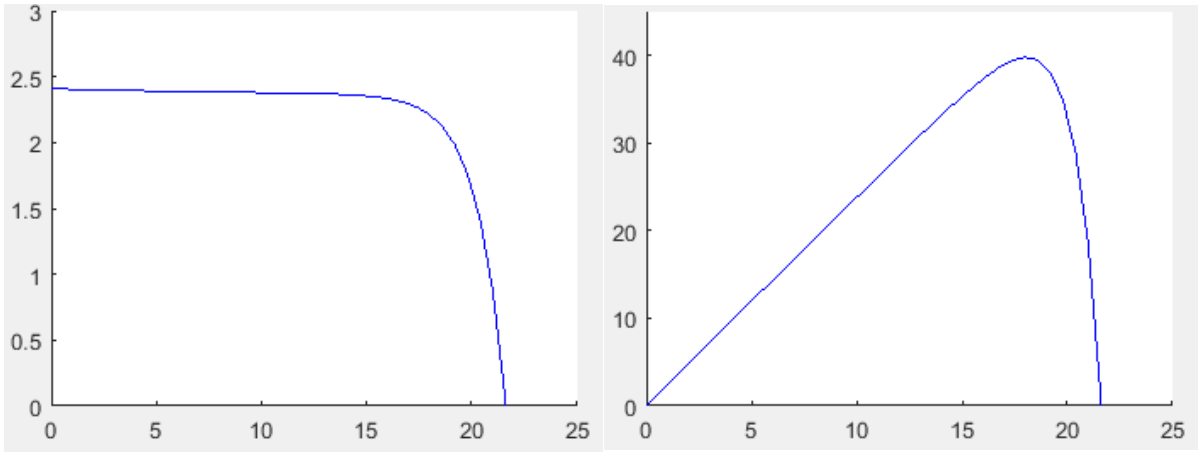

(a) (b)

Figure4.11. (a) I-V and (b) P-V characteristics of STM6-40/36 at STC

Case Study #4: QSMART 95

The extracted ODM parameters for the thin film module QSMART 95 at STC are presented in Table 4.12.While Figure 4.13 shows the obtained I-V and P-V characteristics for the module.

Table4.12. QSMART 95 parameters at STC

(T/G)	Parameters					Error	
	$I_{ph}[A]$	$I_s[\mu A]$	n	$R_s[\Omega]$	$R_{sh}[\Omega]$	RMSE[A]	NRMSE [%]
STC	1.682	2.88	1.926	0.04525	1483	9.344e-4	8.318e-2

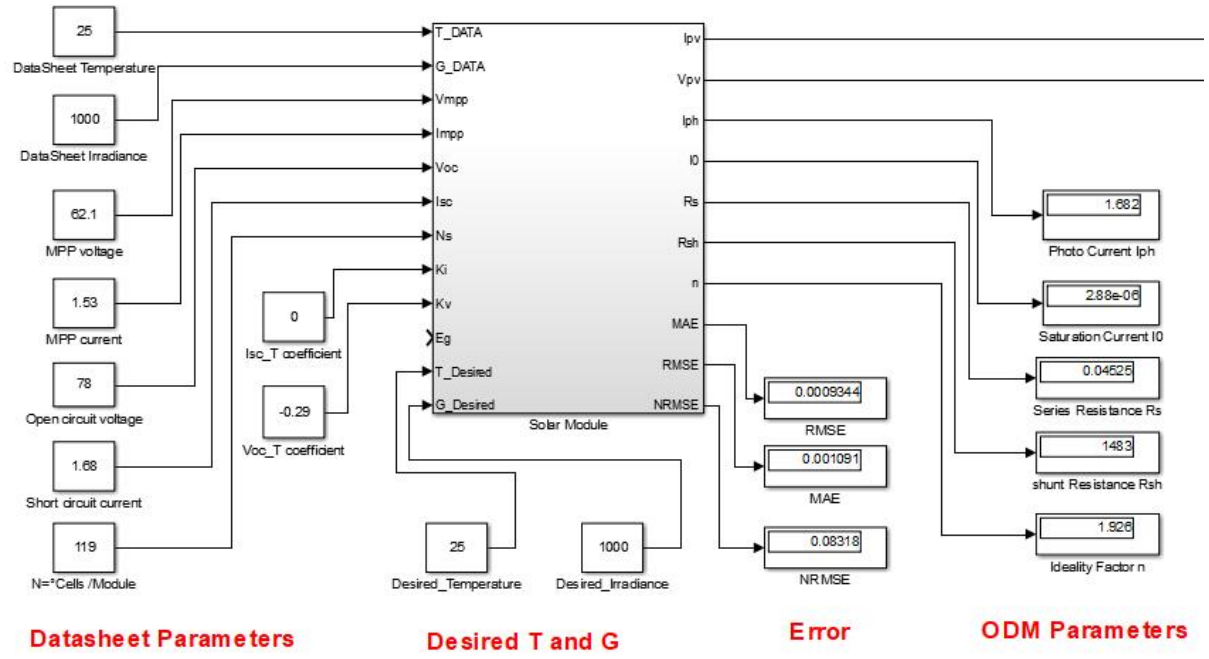

Figure4.12. QSMART 95 simulation results

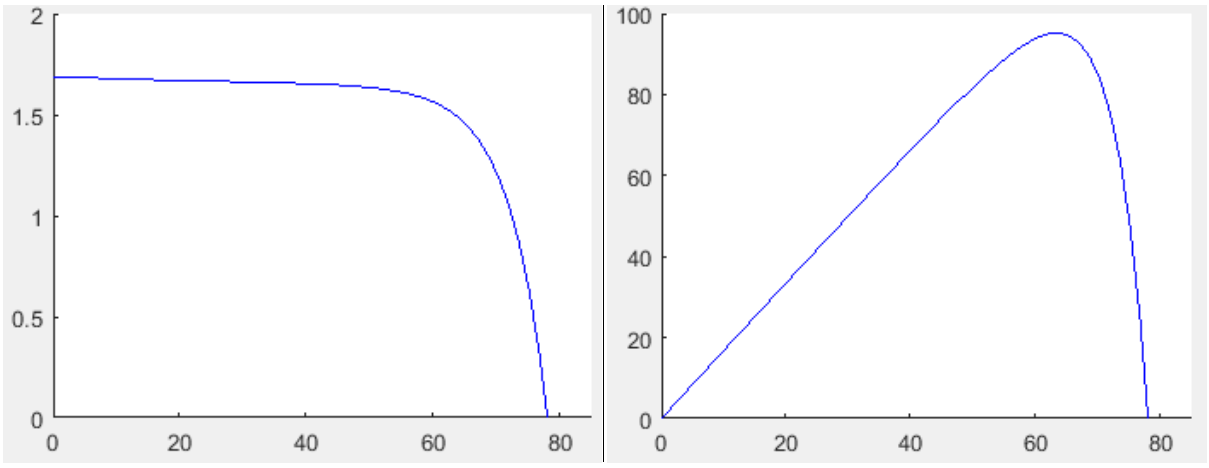

(a) (b)

Figure4.13. QSMART 95 simulation results

4.2 IOB-PSO based ODM Simulation

In this section, the IOB-PSO proposed algorithm is used to extract the parameters of the ODM based on curve fitting method .The algorithm is tested on four PV modules and compared with other algorithms to prove its effectiveness .The simulation is created in MATLAB R2016a and executed on a PC with Intel® Core™ i5-2450M CPU processor @ 2.50GHz, 4GB RAM, under Windows 10 64-bit OS.

The search ranges used in the optimization of the five parameters are the same as the ODM - GWO simulation ranges.

The IOB-PSO parameters are shown in Table 4.13.

Table4.13.IOB-PSO parameters

Parameters	Value
Cognitive factor c1	1.5
Social factor c2	2.0
Inertia weight w	[0.2, 0.9]
Random values r1, r2	[0, 1]
No. of particles	30
Maximum iteration	1000

The IOB-PSO algorithm is used to extract parameters for the different PV modules. The electrical specifications of the utilized modules are described in Table 4.14.

Table4.14.Electrical specifications of the PV modules

Module	Type	N_s	Temperature [°c]	Irradiance [w/m^2]
STM6-40/36	Mono-crystalline	36	51	NA
STP6-120 /36	Poly-crystalline	36	55	NA
Photowatt-PWP201	Poly-crystalline	36	45	1000
BP MSX 120	Poly-crystalline	72	40	300

NA: not available

Case Study #1: STM6-40/36

The mono-crystalline STM6-40/36 module I-V experimental data [24] measured at T=51°c is processed in the proposed algorithm. The extracted ODM parameters are compared with other methods results and tabulated in Table 4.15.

Table4.15. STM6-40/36 extracted parameters achieved by different methods.

Methods	Parameters					Error
	$I_{ph}[A]$	$I_s[\mu A]$	n	$R_s[\Omega]$	$R_{sh}[\Omega]$	RMSE[A]
ABC [25]	1.50	1.6644	1.4866	4.99	15.206	1.8379e-3
CIABC [25]	1.6642	1.6760	1.4976	4.40	15.617	1.819e-3
CSA [24]	1.663969	2.0000	1.533497	2.912981	15.840727	1.79436368e-3
ImCSA [24]	1.663971	2.0000	1.533499	2.913631	15.840511	1.79436329e-3
IOB-PSO*	1.663	2.884351	1.57	0.001479	598.735396	1.7723e-3

* Proposed method

The RMSE error due the proposed IOB-PSO is the least .Thus, the results obtained using it are the best. Therefore its efficiency on extracting the model parameters is proved.

Using the extracted parameters the I-V and P-V curves of the STM6-40/36 module were plotted, they are presented in Figure 4.14.

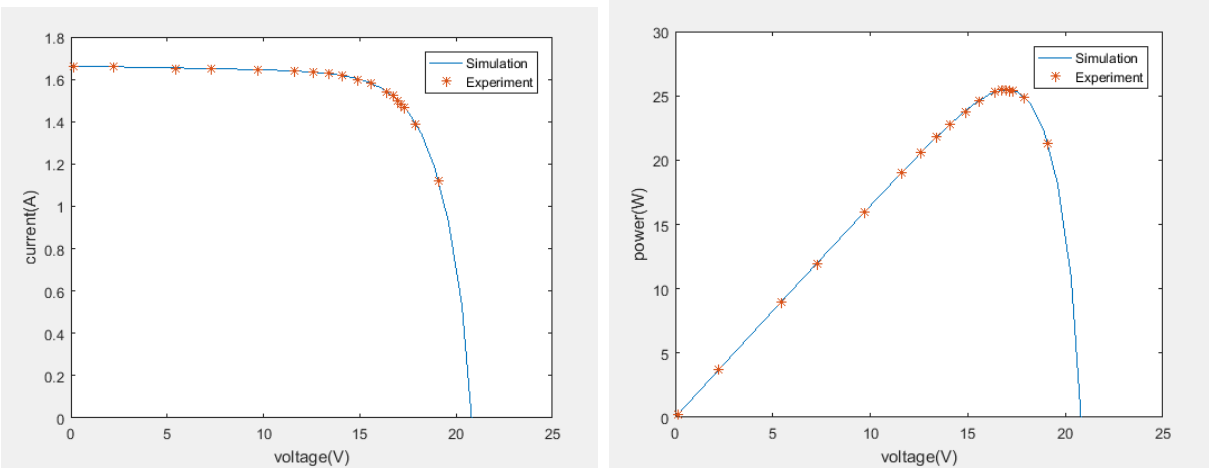

Figure4.14. Comparison between I-V and P-V experimental data and simulated data for the STM6-40/36 module

The simulated curves highly match the measured data which proves the reliability of the IOB-PSO algorithm.

Figure 4.15 presents the convergence curve of the IOB-PSO method for this module; it can be noticed that the convergence is very fast. The algorithm reached the optimal solution within 430 iterations in an execution time of 19.0017 s, which proves the speed of the proposed IOB-PSO method.

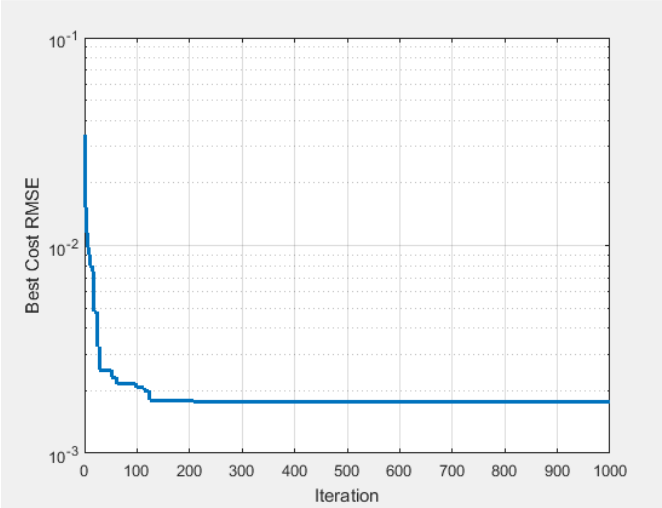

Figure4.15. Convergence curve of the IOB-PSO

Case Study #2: STP6-120 /36 and Photowatt-PWP201

The IOB-PSO is tested again for two poly-crystalline modules .The I-V data was measured under temperatures T=55°c for the STP6-120/36 module and T=45°c for the Photowatt-PWP201 module [24]. The obtained results are presented and compared with other published methods in Tables 4.16, 4.17.

Using the identified parameters the PV characteristics of the two modules were constructed and then compared with the experimental curves in Figure 4.16.

Table4.16. STP6-120 /36 extracted parameters achieved by different methods.

Methods	Parameters				Error	
	I_{ph}[A]	I_s[μA]	n	R_s[Ω]	R_{sh}[Ω]	RMSE[A]
ABC [25], [24]	7.476291	1.20	1.206992	4.91	9.70	1.9174e-2
CIABC [25], [24]	7.484126	1.29	1.214854	5.1	9.89	1.6286553e-2
CSA [24]	7.476291	1.00	1.197733	5.387310	10.00	1.5865806e-2
ImCSA [24]	7.482778	1.00	1.197729	5.386970	10.00	1.5865799e-2
IOB-PSO*	7.457000	1.280217	1.22	0.188154	1499.840439	1.5654e-2

* Proposed method

Table4.17. Photowatt-PWP201 extracted parameters achieved by different methods.

Methods	Parameters					Error
	$I_{ph}[A]$	$I_s[\mu A]$	n	$R_s[\Omega]$	$R_{sh}[\Omega]$	RMSE[A]
CPSO [26], [24]	1.0286	8.3010	1.451194	1.0755	1850.1	3.5e-3
PS [27], [24]	1.0313	3.1756	1.341358	1.2053	714.2857	1.18e-2
SA [28], [24]	1.0331	3.6642	1.356142	1.1989	833.3333	2.7e-3
CARO [29]	1.03185	3.28401	1.35453	1.20556	841.3213	2.427e-3
IOB-PSO*	1.030	3.495668	1.35	1.200877	986.306335	2.4251e-3

* Proposed method

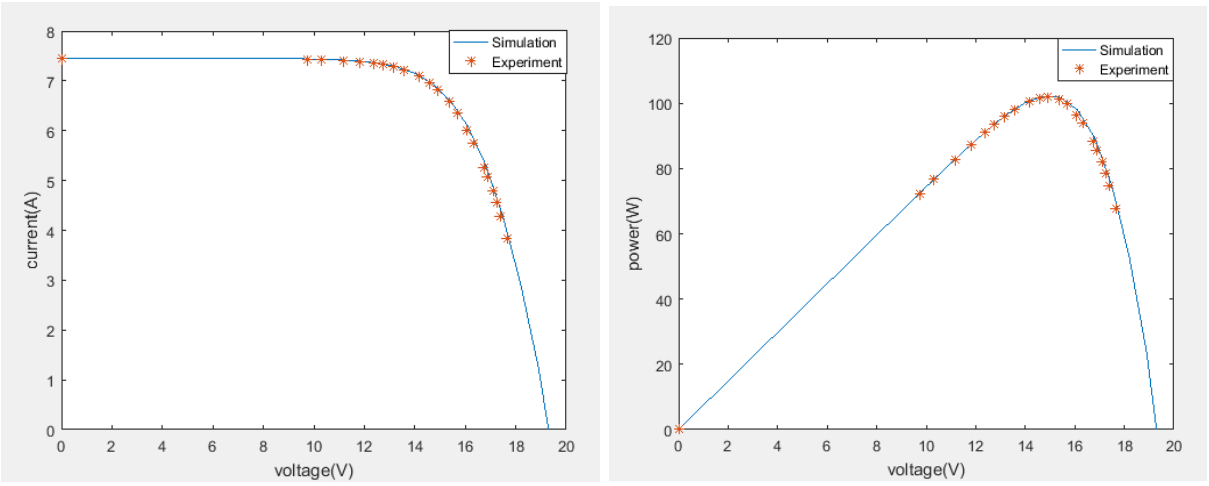

(a)

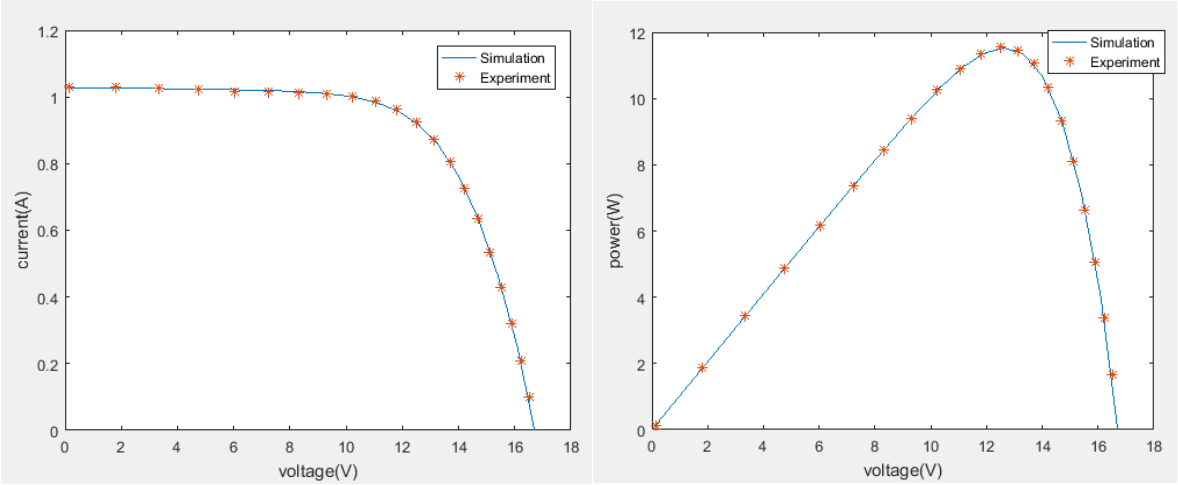

(b)

Figure4.16. Comparison between I-V and P-V experimental data and simulated data for (a) STP6-120/36 module and (b) Photowatt-PWP201 module.

The accuracy of the extracted parameters can be seen in the simulated I-V and P-V characteristics (Figure 4.16). It is noticed that the proposed IOB-PSO algorithm outperformed the compared algorithms and extracted accurately the five parameters for the two modules.

In Figure 4.17 the convergence curves of both modules are presented, for the STP6-120/36 module, the optimal solution is reached within 987 iterations (46.14225s), while for the Photowatt-PWP201 module within 613 iterations (27.585s). That indicates that the proposed IOB-PSO has a very fast convergence speed.

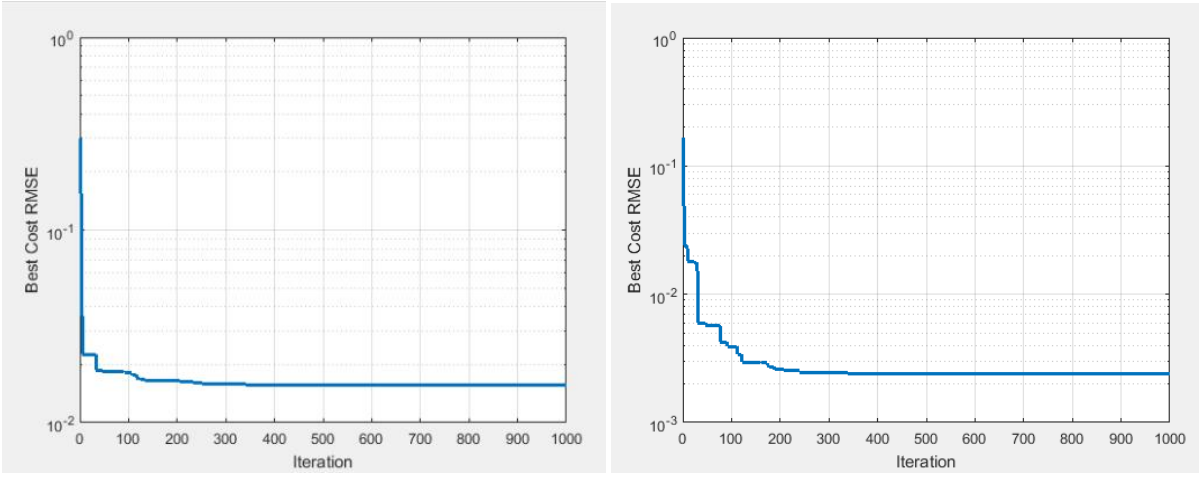

(a) (b)

Figure4.17. Convergence curves of the IOB-PSO (a) STP6-120 /36 (b) Photowatt-PWP201

Case Study #3: BP MSX 120

The I-V experimental data of the BP MSX 120 module [23] measured at T=40°c and G=300 w/m^2 is processed in the proposed IOB-PSO algorithm .The identified ODM parameters are presented in Table 4.18.

Using the extracted parameters the I-V and P-V curves are simulated, and then compared with the measured data points as shown in Figure 4.18.

Figure 4.19 shows the convergence curve of the IOB-PSO for this module.

Table4.18. The IOB-PSO extracted parameters of the BP MSX 120 module

T (°c)	G (w/m^2)	Parameters					Error
		I_{ph}[A]	I_s[μA]	n	R_s[Ω]	R_{sh}[Ω]	RMSE[A]
40	300	1.18	0.10428	1.25	1.477931	1498.807	5.0036e-3

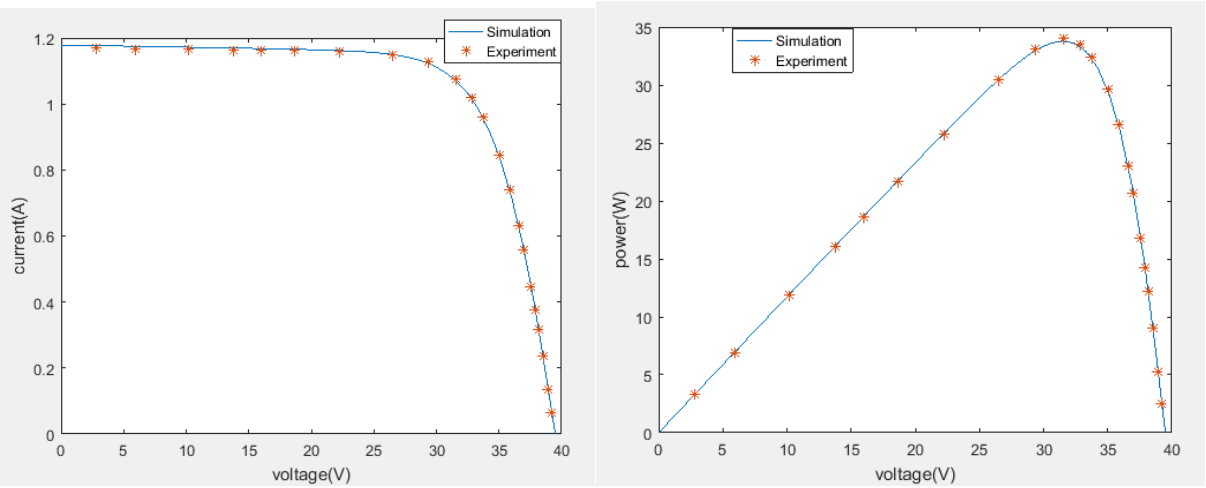

Figure4.18. Comparison between I-V and P-V experimental data and simulated data for the BP MSX 120 module

The measured data points are compatible with the simulated I-V and P-V curves (Figure 4.18). Thus, the proposed IOB-PSO algorithm extracted accurately the five parameters for the BP MSX 120 module.

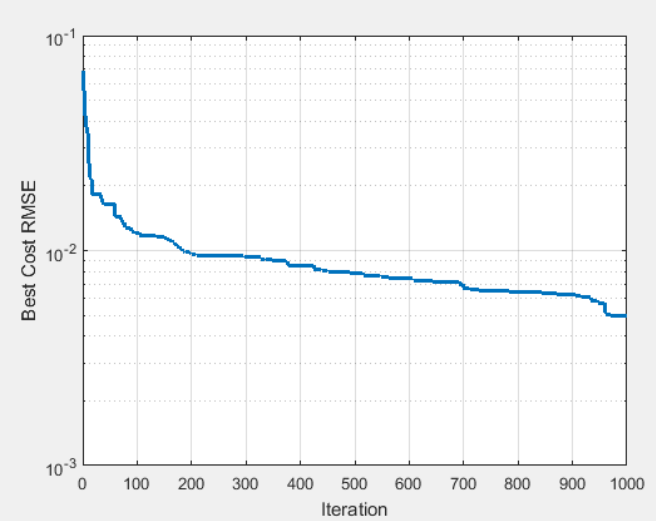

Figure4.19. Convergence curve of IOB-PSO

4.3 Simulation versus Measurement

In this section, the simulated PV characteristics based only on the datasheet information for the two multi-crystalline modules BP MSX 120 and STP050D-12/MEA are compared with the experimental measured data at the given environmental conditions to validate the developed GWO based ODM PV simulator.

Case Study #1:

The previously simulated PV characteristics of the BP MSX 120 module at T=40°c and G=300 w/m^2 using the GWO based ODM PV simulator are compared with the module's measured data points [23]. The comparison results are presented in Figure 4.20.

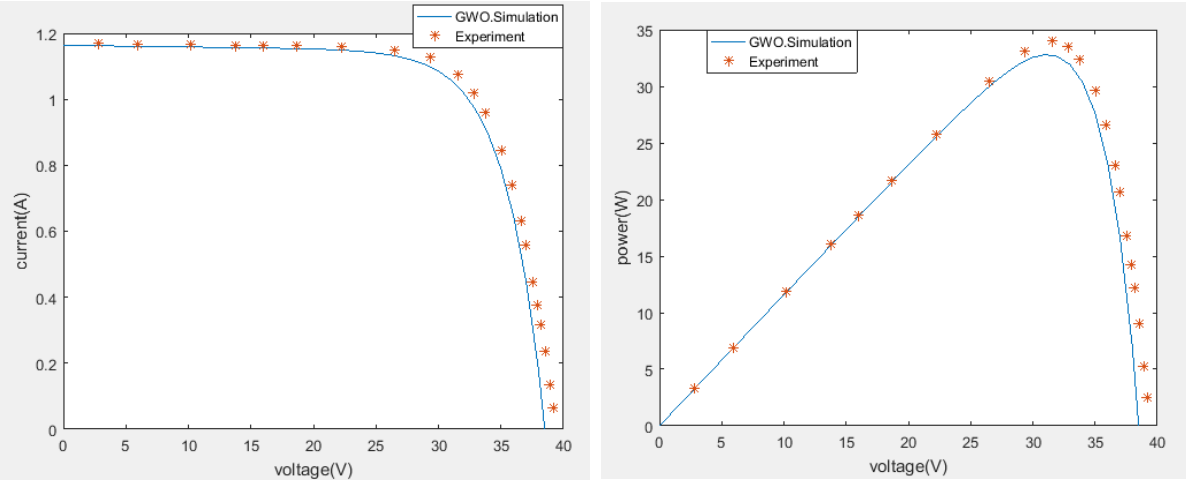

Figure4.20. Experimental versus GWO Simulation I-V and P-V characteristics

Table4.19. Comparison of Experimental values and GWO simulation model values at MPP

Parameters	Experimental Parameters	Parameters from the simulation of the model	Relative error (%)
V_{mpp}[V]	31.6	31.0	1.89873418
I_{mpp}[A]	1.0768	1.0580	1.74591382
P_{max}[W]	34.0269	32.7984	3.61037885

The results obtained by comparing the experimental curves and the GWO model simulated PV characteristics demonstrates an acceptable accuracy of the proposed GWO based ODM PV simulator.

Case Study #2: STP050D-12/MEA

The PV characteristics of the poly-crystalline STP050D-12/MEA module are simulated at T=45.57°c and G= 632 w/m^2 using the GWO based ODM PV simulator .The obtained results are given in Table 4.21 and Figures 4.21 , 4.22 .The computed errors are: RMSE= 1.327e-3 and NRMSE= 7.282e-2 .

Table4.20. STP050D-12/MEA datasheet Parameters

Module	Type	$V_{mpp}[V]$	$I_{mpp}[V]$	$V_{oc}[V]$	$I_{sc}[V]$	N_s	STC (T/G)
STP050D-12/MEA	Poly-crystalline	17.4	2.93	21.8	3.13	36	25°c/1000w/m^2

Table4.21. STP050D-12/MEA extracted parameters

T [°c]	G [w/m^2]	Parameters				
		$I_{ph}[A]$	$I_s[\mu A]$	n	$R_s[\Omega]$	$R_{sh}[\Omega]$
45.57	632	1.986	1.326	1.497	0.1024	1497

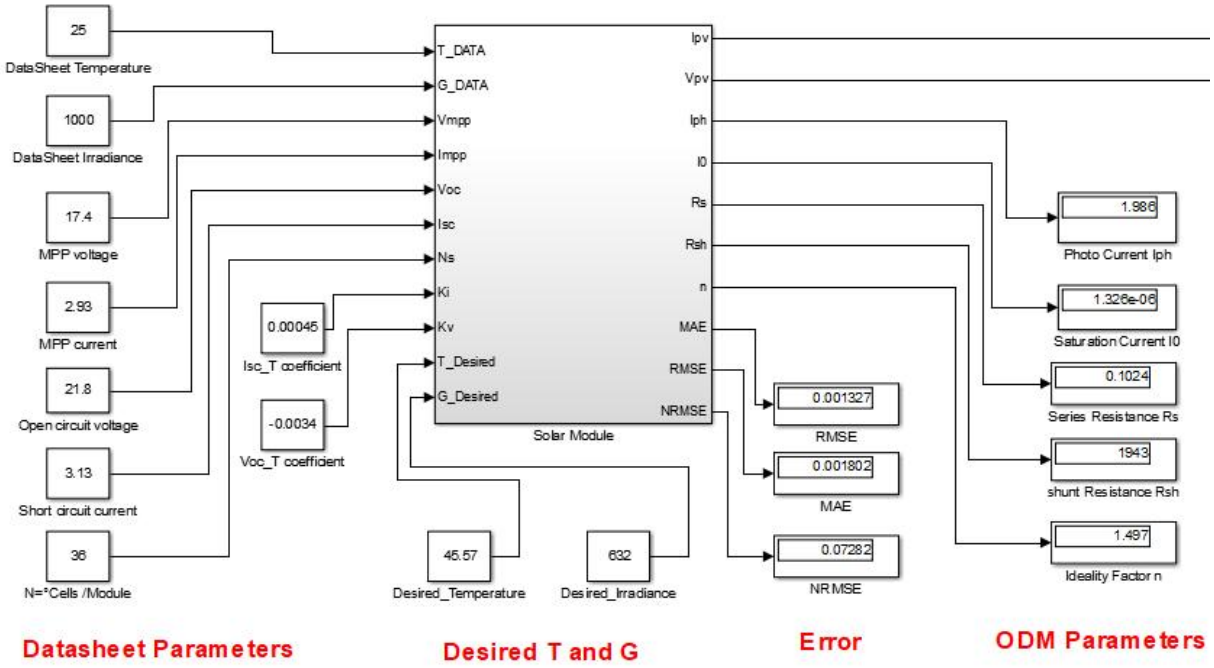

Figure4.21. STP050D-12/MEA simulation results at T=45.57°c and G = 632 w/m^2

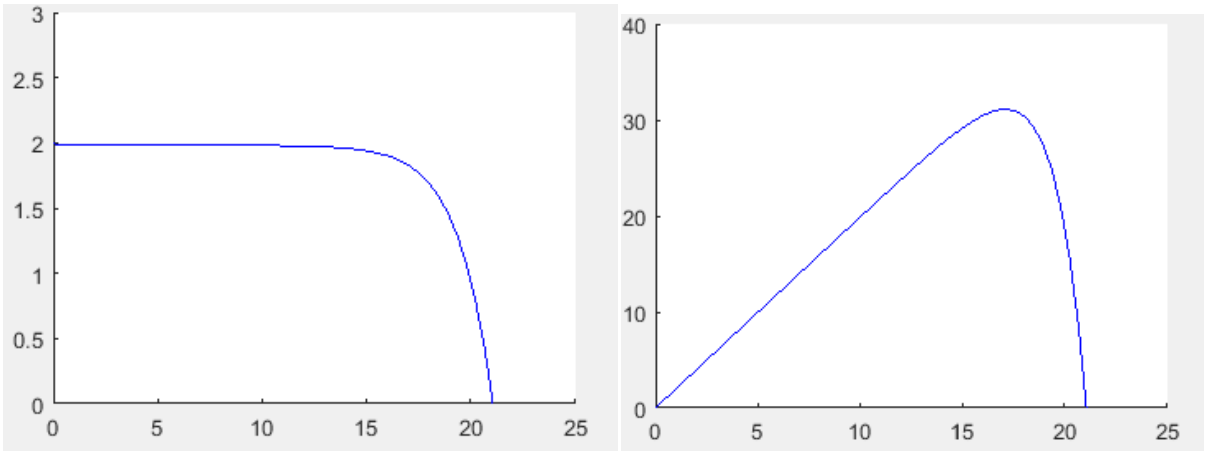

(a) (b)

Figure4.22. (a) I-V and (b) P-V characteristics of STP050D-12/MEA module at T=45.57°c and G = 632 w/m^2

Figure 4.23 presents the experimental I-V and P-V characteristics obtained for the STP050D-12/MEA module at T=45.57°c and G = 632 w/m^2 using the PV panel characterization platform developed in our research laboratory [30].

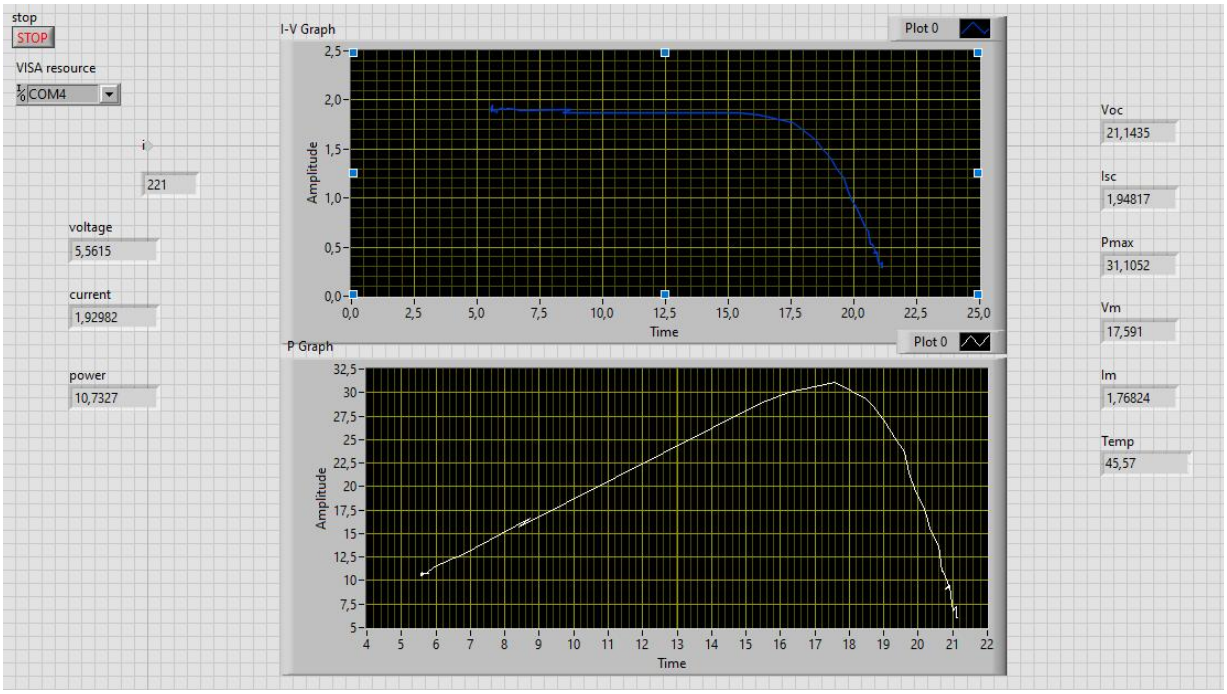

Figure4.23. Experimental I-V and P-V characteristics

The simulated characteristics are compared with the module's experimental data [30]. The comparison results are presented in Figure 4.24 and Table 4.22.

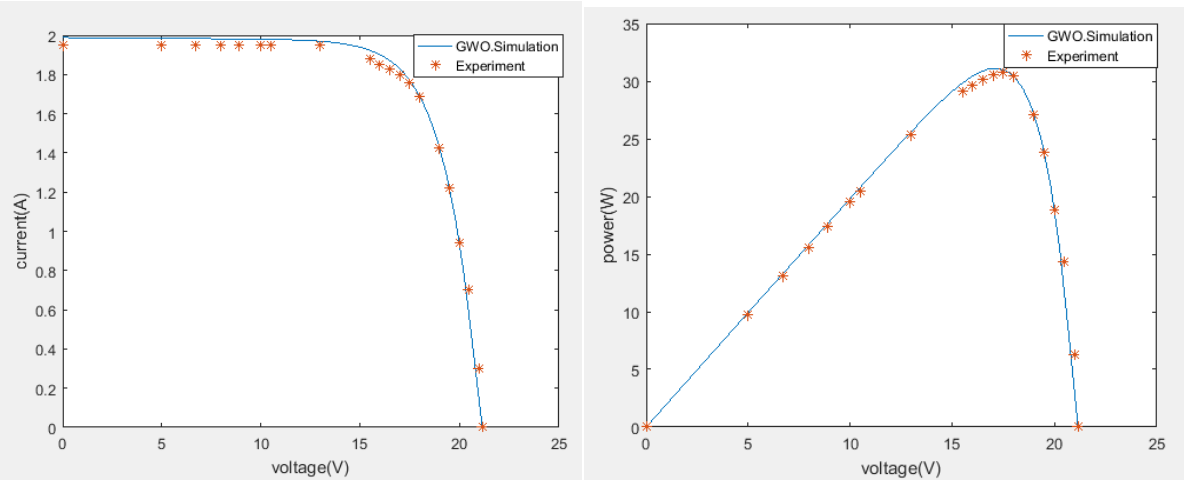

Figure4.24. Experimental versus GWO Simulation I-V and P-V characteristics

Table 4.22. Comparison of Experimental and simulation model values

Parameters	Experimental Parameters	Parameters from the simulation of the model	Relative error (%)
$V_{mpp}[V]$	17.591	17.16	2.450116537
$I_{mpp}[A]$	1.76824	1.8138	2.576573316
$P_{max}[W]$	31.1052	31.1242	0.06108303435
$V_{oc}[V]$	21.1435	21.15	0.03074230851
$I_{sc}[A]$	1.94817	1.9926	2.280601796

It can be noticed that the measured data points obtained in our laboratory for the STP050D-12/MEA module are compatible with the simulated curves. Thus, the obtained I-V and P-V characteristics for the STP050D-12/MEA module based only on the datasheet information using the GWO based ODM PV simulator gives good results.

CHAPTER FIVE:

Conclusions and Future Work

Chapter 5

Conclusions and Future Work

PV cell characterization is a hot research topic in renewable energy. Obtaining the most accurate I-V and P-V characteristics has been the main purpose of this project. As an introductory background to the research subject, the importance of solar energy and photovoltaic power generation has been presented; in addition, the main operation principles of PV systems have been discussed with the effect of the changing environmental conditions.

In this work, the first intended objective is to find an efficient method for obtaining the I-V and P-V Characteristics of a PV module based on the one diode model using the information provided by the manufacturers. However, not all (five) parameters are available in the datasheet. Thus, the simulation has been associated with the developed algorithm that permits finding the appropriate value of the needed parameters. Due to the fact of the I-V equation being of non-explicit nature, finding an analytic solution is quiet difficult. However, using numerical methods is a simpler way for extracting the unknown parameters but its main drawback is the non-accuracy of the obtained results. Therefore, optimization algorithms have been introduced in this work for the identification of the model parameters. Optimization methods, specifically, metaheuristics algorithms based on artificial intelligence have been proved to be very efficient in the extraction of the optimal solutions for the PV model equation.

Two metaheuristics algorithms were employed in this project, the first one is the grey wolf optimization (GWO).This algorithm was implemented using the SIMULINK for extracting the five parameters based only in the three critical I-V points information provided in the datasheet which are the open circuit point ($V_{oc}, 0$), the short circuit point ($0, I_{sc}$), and the maximum power point (V_{mpp}, I_{mpp}).Furthermore, this method has been enhanced to provide the parameters under different environmental conditions. The developed ODM-GWO simulation was tested for various PV modules, under different temperatures and irradiances. The obtained I-V and P-V curves were compared to the characteristics provided in the datasheet. Moreover, the BP MSX 120 and the STP050D-12/MEA modules simulated curves were compared to the experimental I-V data. The measured data points have conformed to the obtained curves; thus, the good accuracy of the developed PV simulator was demonstrated.

The second aim of this project was to develop an algorithm for PV parameters identification from measured I-V data. The proposed method is an improved opposition based particle swarm optimization; this algorithm was tested using the experimental I-V data that were acquired at different working conditions for various PV modules. The obtained results were compared with other methods outcomes provided in the references, this algorithm have showed a satisfying estimation of the five parameters extracted with minimum errors. Furthermore, the PV characteristics were plotted using the extracted parameters and compared with the experimental data. The simulated curves are found to be well-suited with the corresponding measured data, thus, the performance of IOB-PSO algorithm was proved to be good. Adding to the fact that these proposed algorithms have provided optimal results with an acceptable accuracy, the time taking by the ODM-GWO process is less than 10 seconds and for the IOB-PSO is less than 50 seconds.

Finally, based on the results obtained for the proposed approaches, it can be concluded that the main aim of this work is well achieved for solving the photovoltaic characterization problem.

To conclude, it can be noted that the following points must be considered for enhancing the characterization of PV modules in future work:

- The output of current and voltage in the PV system characteristics are closely related to the solar irradiance, ambient temperature and wind speed during the real operation process. Therefore, future work will include improving the PV simulator by considering all these environmental factors. Moreover, introducing the cell temperature as a parameter to be determined can lead to better identification of PV parameters.
- In cases where experimental I-V data are used for parameter estimation of solar PV modules, using data sets with larger number of I-V data points can lead to results of higher accuracy. However, computational time increases.
- Control parameters of metaheuristic optimization algorithms significantly affect their computational behavior. The suitable values of control parameters are different for different problems. For each optimization problem, the suitable values of control parameters must be tuned.

Bibliography

[1] https://www.bbvaopenmind.com/en/articles/current-challenges-in-energy/

[2] https://www.herox.com/blog/222-a-promising-future-solar-energy-to-become-cheapest

[3]https://earthobservatory.nasa.gov/features/EnergyBalance/

[4] World Energy Resources: Solar World Energy Council 2013 Available:https://www.worldenergy.org/assets/images/imported/2013/10/WER_2013_8_Solar_revise d.pdf

[5] https://solargis.com/maps-and-gis-data/download/world

[6] IEA, "International energy agency." in International Energy Agency, 2020. [Online].

[7] IRENA_RE_Capacity_Statistics_2020

[8] E. Batzelis, "Non-iterative methods for the extraction of the single-diode model parameters of photovoltaic modules: A review and comparative assessment," Energies, vol. 12, no. 3, p. 358, Jan. 2019.

[9] https://www.ecomena.org/renewables-algeria/

[10] Centre de Développement des Energies Renouvelables (cder.dz)

[11] Ashrafun Nushra Oishi, Meer Shadman Shafkat Tanjim, M. Tanseer Ali. "Loss Analysis of Market Available Solar Cells and Possible Solutions ". September 2019

[12] Abdullateef A. Jadallah, Abduljabbar O. Hanfesh, Tabarek H. Jebur ." Design, Fabrication, Testing And Simulation Of a Modern Glass To Glass Photovoltaic Module In Iraq". Journal of Engineering Science and Technology Vol. 13, No. 9 (2018) 2750 - 2764

[13] V.Franzitta, A. Orioli , A. Di Gangi." Assessment of the Usability and Accuracy of the Simplified One-Diode Models for Photovoltaic Modules "

[14] https://mathworld.wolfram.com/GlobalOptimization.html

[15] S. Mirjalili, S. M. Mirjalili, and A. Lewis, "Grey wolf optimizer,"Adv. Eng. Software, vol. 69 , 2014, pp. 46–61

[16] C. Muro, R. Escobedo, L. Spector, and R. Coppinger, "Wolf-pack (Canis lupus) hunting strategies emerge from simple rules in computational simulations," *Behavioural processes,* vol. 88, pp. 192-197, 2011.

[17] https://www.sciencedirect.com/topics/mathematics/matlab

[18] https://cimss.ssec.wisc.edu/wxwise/class/aos340/spr00/whatismatlab.htm

[19] Using Simulink®Version 6.Simulation and Model-Based Design COPYRIGHT 1990 - 2004 by The MathWorks, Inc
[20] Jordehi, A. Rezaee. "Parameter Estimation of Solar Photovoltaic (PV) Cells: A Review." *Renewable and Sustainable Energy Reviews* 61 (2016): 354–71.
[21] T. Wei, F. Yu, G. Huang, and C. Xu, "A particle-swarm-optimization based parameter extraction routine for three-diode lumped parameter model of organic solar cells," IEEE Electron Device Letters, vol. 40, no. 9, pp. 1511–1514, Sep. 2019.
[22] Stornelli, Muttillo, de Rubeis, and Nardi, "A new simplified fiveparameter estimation method for single-diode model of photovoltaic panels," Energies, vol. 12, no. 22, p. 4271, Nov. 2019
[23] M. Bencherif,B. Nabil.Brahm . " Accurate method for loss parameter extraction of solar panels".
[24] Tong Kang ; Jiangang Yao ; Min Jin ; Shengjie Yang ; ThanhLong Duong . A Novel Improved Cuckoo Search Algorithm for Parameter Estimation of Photovoltaic (PV) Models". April 2018
[25] Oliva, D.; Ewees, A.A.; Aziz, M.A.E.; Hassanien, A.E.; Cisneros, M.P. A chaotic improved artificial bee colony for parameter estimation of photovoltaic cells. *Energies* 2017, *10*, 865
[26] Wei, H.; Cong, J.; Lingyun, X.; Deyun, S. Extracting solar cell model parameters based on chaos particle swarm alogorithm. In Proceedings of the 2011 International Conference on Electric Information and Control engineering (ICEICE), Wuhan, China, 15–17 April 2011; pp. 398–402.
[27] Alhajri, M.F.; El-Naggar, K.M.; Alrashidi, M.R.; Al-Othman, A.K. Optimal extraction of solar cell parameters using pattern search. *Renew. Energy* **2012**, *44*, 238–245.
[28] El-Naggar, K.M.; AlRashidi, M.R.; AlHajri, M.F.; Al-Othman, A.K. Simulated Annealing algorithm for photovoltaic parameters identification. *Sol. Energy* **2012**, *86*, 266-274.
[29] Yuan, X.; He, Y.; Liu, L. Parameter extraction of solar cell models using chaotic asexual reproduction optimization. *Neural Comput. Appl.* **2015**, *26*, 1227–1239.
[30] Habes, A; Amara,A."Design and Implementation of PV panel characterization platform".

THE NEW VALUE FRONTIER

KYOCERA

KC200GT

HIGH EFFICIENCY MULTICRYSTAL
PHOTOVOLTAIC MODULE

UL LISTED

HIGHLIGHTS OF KYOCERA PHOTOVOLTAIC MODULES

Kyocera's advanced cell processing technology and automated production facilities produce a highly efficient multicrystal photovoltaic module.
The conversion efficiency of the Kyocera solar cell is over 16%.
These cells are encapsulated between a tempered glass cover and a pottant with back sheet to provide efficient protection from the severest environmental conditions.
The entire laminate is installed in an anodized aluminum frame to provide structural strength and ease of installation.
Equipped with plug-in connectors.

MODEL
KC200GT

APPLICATIONS

KC200GT is ideal for grid tie system applications.

- Residential roof top systems
- Large commercial grid tie systems
- Water Pumping systems
- High Voltage stand alone systems
- etc.

QUALIFICATIONS

- **MODULE** : UL1703 certified
- **FACTORY** : ISO9001 and ISO 14001

QUALITY ASSURANCE

Kyocera multicrystal photovoltaic modules have passed the following tests.

- Thermal cycling test
- Thermal shock test
- Thermal / Freezing and high humidity cycling test
- Electrical isolation test
- Hail impact test
- Mechanical, wind and twist loading test
- Salt mist test
- Light and water-exposure test
- Field exposure test

LIMITED WARRANTY

※1 year limited warranty on material and workmanship
※20 years limited warranty on power output: For detail, please refer to "category IV" in Warranty issued by Kyocera

(Long term output warranty shall warrant if PV Module(s) exhibits power output of less than 90% of the original minimum rated power specified at the time of sale within 10 years and less than 80% within 20 years after the date of sale to the Customer. The power output values shall be those measured under Kyocera's standard measurement conditions. Regarding the warranty conditions in detail, please refer to Warranty issued by Kyocera)

ELECTRICAL CHARACTERISTICS

Current-Voltage characteristics of Photovoltaic Module KC200GT at various cell temperatures

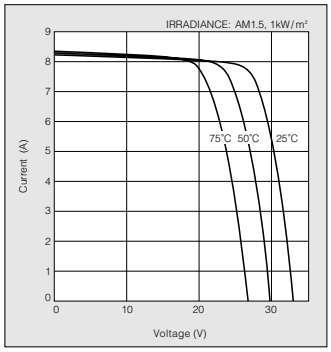

Current-Voltage characteristics of Photovoltaic Module KC200GT at various irradiance levels

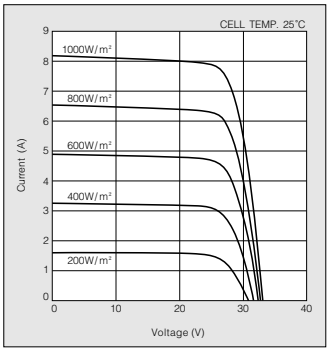

SPECIFICATIONS

KC200GT

Physical Specifications

Unit : mm (in.)

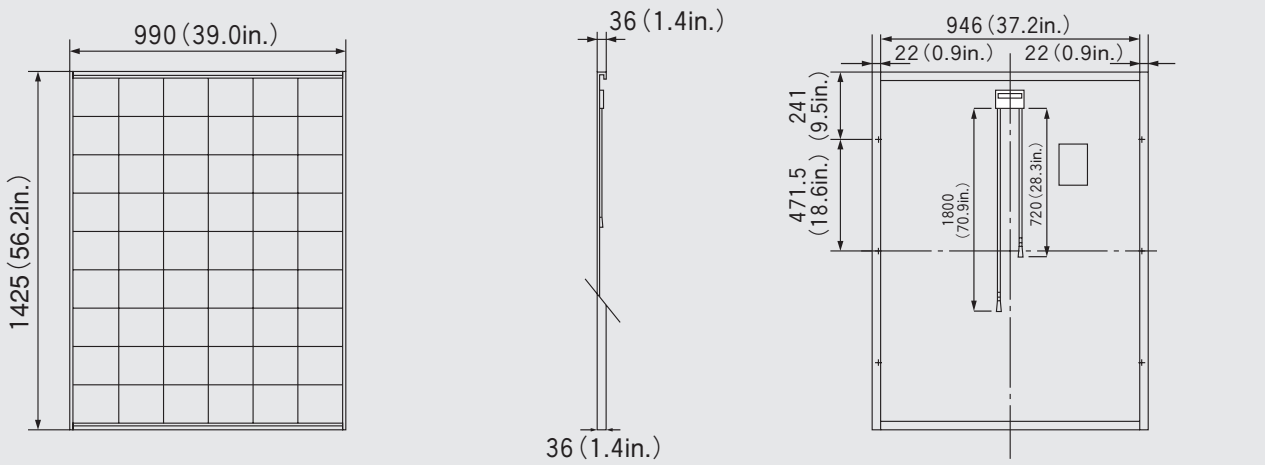

Specifications

Electrical Performance under Standard Test Conditions (*STC)	
Maximum Power (Pmax)	200W (+10%/−5%)
Maximum Power Voltage (Vmpp)	26.3V
Maximum Power Current (Impp)	7.61A
Open Circuit Voltage (Voc)	32.9V
Short Circuit Current (Isc)	8.21A
Max System Voltage	600V
Temperature Coefficient of Voc	-1.23×10^{-1} V/℃
Temperature Coefficient of Isc	3.18×10^{-3} A/℃

*STC : Irradiance 1000W/m², AM1.5 spectrum, module temperture 25℃

Electrical Performance at 800W/m², NOCT, AM1.5	
Maximum Power (Pmax)	142W
Maximum Power Voltage (Vmpp)	23.2V
Maximum Power Current (Impp)	6.13A
Open Circuit Voltage (Voc)	29.9V
Short Circuit Current (Isc)	6.62A

NOCT (Nominal Operating Cell Temperature) : 47℃

Cells	
Number per Module	54

Module Characteristics	
Length × Width × Depth	1425mm(56.2in)×990mm(39.0in)×36mm(1.4in)
Weight	18.5kg(40.7lbs.)
Cable	(+)720mm(28.3in),(-)1800mm(70.9in)

Junction Box Characteristics	
Length × Width × Depth	113.6mm(4.5in)×76mm(3.0in)×9mm(0.4in)
IP Code	IP65

Reduction of Efficiency under Low Irradiance	
Reduction	7.8%

Reduction of efficiency from an irrandiance of 1000W/m² to 200W/m² (module temperature 25℃)

Please contact our office for further information

KYOCERA

KYOCERA Corporation

■ KYOCERA Corporation Headquarters
CORPORATE SOLAR ENERGY DIVISION
6 Takeda Tobadono-cho
Fushimi-ku, Kyoto
612-8501, Japan
TEL:(81)75-604-3476 FAX:(81)75-604-3475
http://www.kyocera.com

● KYOCERA Solar, Inc.
7812 East Acoma Drive
Scottsdale, AZ 85260, USA
TEL:(1)480-948-8003 or (800)223-9580 FAX:(1)480-483-6431
http://www.kyocerasolar.com

● KYOCERA Solar do Brasil Ltda.
Av. Guignard 661, Loja A
22790-200, Recreio dos Bandeirantes, Rio de Janeiro, Brazil
TEL:(55)21-2437-8525 FAX:(55)21-2437-2338
http://www.kyocerasolar.com.br

● KYOCERA Solar Pty Ltd.
Level 3, 6-10 Talavera Road, North Ryde
N.S.W. 2113, Australia
TEL:(61)2-9870-3948 FAX:(61)2-9888-9588
http://www.kyocerasolar.com.au/

● KYOCERA Fineceramics GmbH
Fritz Muller strasse 107, D-73730 Esslingen, Germany
TEL:(49)711-93934-917 FAX:(49)711-93934-950
http://www.kyocerasolar.de/

● KYOCERA Asia Pacific Pte. Ltd.
298 Tiong Bahru Road, #13-03/05
Central Plaza, Singapore 168730
TEL:(65)6271-0500 FAX:(65)6271-0600

● KYOCERA Asia Pacific Ltd.
Room 801-802, Tower 1 South Seas Centre, 75 Mody Road,
Tsimshatsui East, Kowloon, Hong Kong
TEL:(852)2-7237183 FAX:(852)2-7244501

● KYOCERA Asia Pacific Ltd. Taipei Office
10 Fl., No.66, Nanking West Road, Taipei, Taiwan
TEL:(886)2-2555-3609 FAX:(886)2-2559-4131

● KYOCERA(Tianjin) Sales & Trading Corporation
19F, Tower C HeQiao Building 8A GuangHua Rd.,
Chao Yang District, Beijing 100026, China
TEL:(86)10-6583-2270 FAX:(86)10-6583-2250

Schutten solar
blue sky . green life

Strengths

- +5 Toleance 0~+5
- High transmission,low Iron Tempered Glass
- Plug&Play Connectors
- Bypass Diodes Protection
- Salt Mist And Ammonia Resistance Test

Warranty

- 12 Manufacturing 12 Years
- Power Production 90%:12years 80%:25years

Insurance

- Insured By CHUBB

Certificates

CE ISO IEC TÜV NORD MCS Clean Energy Council J-PEC CQC

IEC 61215 , 61730

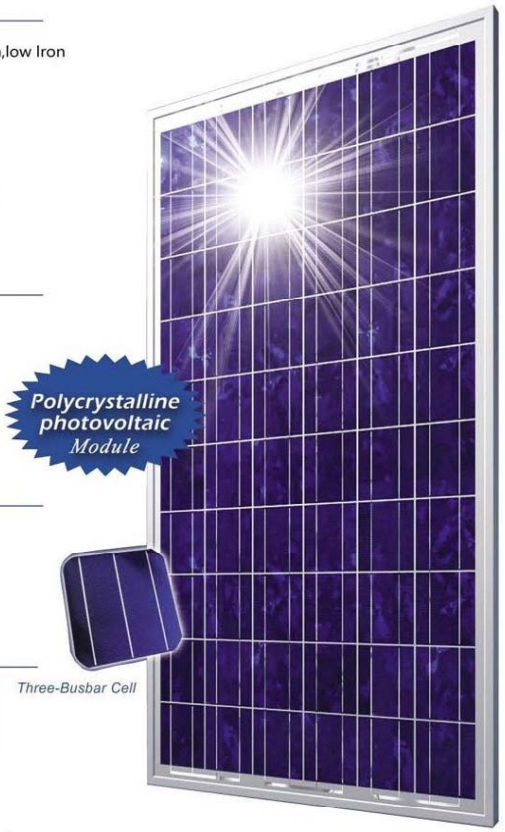

Electrical Characteristics		Mono Crystalline				Poly Crystalline		
Module Type	Unit	STM5-20/36	STM6-40/36	STM6-80/36	STM5-120/48	STP-50/36	STP6-80/40	STP6-120/36
External Dimensions	mm	540x290x25	670x420x25	770x670x30	1070x808x30	670x540x25	850x670x30	1473x670x30
Weight	Kg	1.6	5	6.8	8.8	5.5	7.2	8.8
Rated Power ar STC	W	20	40	80	120	50	80	120
Power Tolerance	W	± 3%	± 3%	± 3%	± 3%	± 3%	± 3%	± 3%
Power Maximum at STC	W	20	40	80	120	50	80	120
Cell Effciency	%	15.90- 16.10	15.90- 16.10	15.90- 16.10	15.90- 16.10	15.5-15.7	15.5-15.7	15.5-15.7
Open Circuit Voltage (Voc)	V	21.6	21.6	21.6	28.8	21.6	24.96	21.24
Short Circuit Current (Isc)	A	1.22	2.36	4.82	5.56	3.3	4.18	7.33
Maximum Power Voltage (Vmp)	V	18	18	18	24.1	17.3	20.92	18
Maximum Power Current (Imp)	A	1.12	2.23	4.45	4.98	2.9	3.83	6.67
Maximum System Voltage DC	V	1000						
Maximum Series Fuse Rating	A	12						

Q.CELLS
YIELD SECURITY

- ANTI PID TECHNOLOGY (APT)
- ADDITIONAL POWER BOOST (APB)
- 360° EFFICIENCY (TDE)

CIGS SOLAR MODULE

Q.SMART 75-95

Generation 1.3 - Efficiency and esthetics have a new name

With up to 13.4 %, our CIGS solar modules of the Q.SMART series are the most efficient thin-film modules on the market. The outstanding low-light behaviour as well as the extra power due to positive sorting and light soaking effect make them ideal for challenging installations. Q.SMART is our all-rounder for private rooftops and facades.

THE NEW Q-CELLS GENERATION

- World's best efficiencies up to 13.4 %: **Highest yields per installed area.**
- Anti PID Technology (APT)[1]: **No power loss caused by potential induced degradation.**
- Outstanding diffuse and low-light behaviour for 360° Efficiency (TDE): **High yields even in challenging roof expositions - north, west, south, east.**

THE PROVEN Q-CELLS VALUES

- Additional Power Boost (APB) with up to 15 % additional output due to positive sorting (+5 / -0W) and light soaking effect: **More power for your money.**
- Black surface and black aluminum frame: **Excellent visual appearance.**
- Tested for 5,400 Pa: **Strong in every weather condition.**
- 25 years linear performance warranty, 10 years product warranty[2], even for installations <30 kWp: **Secure investment.**

THE IDEAL SOLUTION FOR:

ROOFTOP ARRAYS ON RESIDENTIAL BUILDINGS

FACADE INSTALLATIONS

[1] APT test conditions: Cells at -600 V relative to frame, wet module surface, 25 °C, 300 h

[2] Performance warranty: min. 100 % of nominal power in the first 3 years; max. 0.7 % degradation per year from year 4; min. 85 % of nominal power after 25 years. Full product and performance warranties are subject to registration, and are in accordance with the valid regional warranty terms.

Q.CELLS

MECHANICAL SPECIFICATION

Length	1196 (+1/-0.5) mm
Width	636 (+1/-0.5) mm
Height	36 mm (incl. junction box and frame)
Weight	14.5 kg
Front Cover	4 mm tempered low iron glass
Back Cover	3 mm float glass
Frame	Black anodized aluminium
Cell Type	CIGS [Cu(In, Ga) Se_2]
Junction box	Protection class IP 65, with 1 bypass diode (3 A) 66 x 54 x 15 mm^3
Cable type	Solar cable 2.5 mm^2; (+) 855 (+30/-0) mm; (–) 735 (+30/-0) mm
Connector	MC4

TECHNICAL DRAWING

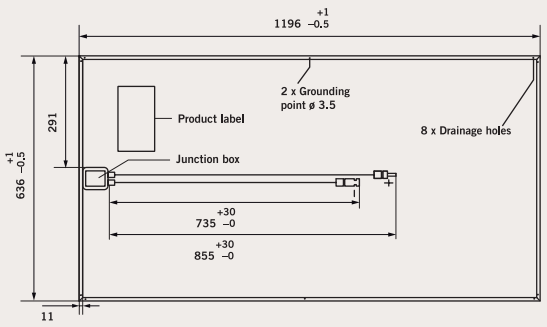

ELECTRICAL CHARACTERISTICS

PERFORMANCE AT STANDARD TEST CONDITIONS (STC: 1000 W/m², 25 °C, AM 1.5 SPECTRUM)[1]

POWER CLASS			75	80	85	90	95
Nominal Power (+5/-0 Wp)	P_{MAX}	[W]	75.0	80.0	85.0	90.0	95.0
Short Circuit Current	I_{SC}	[A]	1.66	1.66	1.67	1.67	1.68
Open Circuit Voltage	V_{OC}	[V]	74.4	74.5	75.2	76.5	78.0
Current at Maximum Power	I_{MPP}	[A]	1.40	1.42	1.44	1.48	1.53
Voltage at Maximum Power	V_{MPP}	[V]	53.6	56.4	59.0	60.8	62.1
Nominal Efficiency	η	[%]	≥9.9	≥10.5	≥11.2	≥11.8	≥12.5

PERFORMANCE AT NORMAL OPERATING CELL TEMPERATURE (NOCT: 800 W/m², 51 ±2 °C, AM 1.5 SPECTRUM)

POWER CLASS			75	80	85	90	95
Nominal Power	P_{MAX}	[W]	54.2	57.8	61.4	65.1	68.7
Short Circuit Current	I_{SC}	[A]	1.33	1.33	1.33	1.33	1.34
Open Circuit Voltage	V_{OC}	[V]	67.7	67.8	68.4	69.6	71.0
Current at Maximum Power	I_{MPP}	[A]	1.11	1.13	1.14	1.18	1.22
Voltage at Maximum Power	V_{MPP}	[V]	48.6	51.2	53.5	55.2	56.3

[1] Measurement accuracy: ±10 %. All STC measurements based on pre-treatement of modules with 1 hour light soak (1000 W/m² [1 kWh/m²], in open circuit) followed by cool down to 25 °C. For the system conception, please take into account the typical relative V_{OC} and V_{MPP} power increase of 2.5 % after 215 kWh/m² light soaking. This power boost is not included in the nominal values of this data sheet.

PERFORMANCE AT LOW IRRADIANCE

The typical relative change in module efficiency (at nominal power) at an irradiance of 200 W/m² in relation to 1000 W/m² (both at 25 °C and AM 1.5 spectrum) is -4.0 % rel.

CHARACTERISTICS AT DIFFERENT TEMPERATURES AND IRRADIANCES

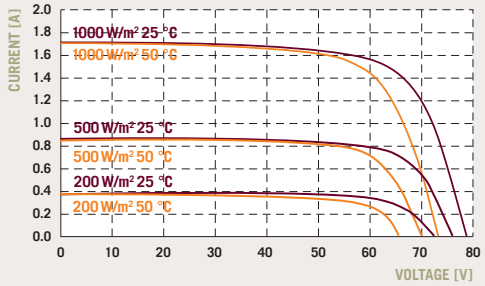

TEMPERATURE COEFFICIENTS (AT 1000 W/m², AM 1.5 SPECTRUM)

Temperature Coefficient of I_{SC}	α	[%/K]	+ 0.00 ±0.04	**Temperature Coefficient of V_{OC}**	β	[%/K]	−0.29 ±0.04
Temperature Coefficient of P_{MAX}	γ	[%/K]	−0.38 ±0.04				

PROPERTIES FOR SYSTEM DESIGN

Maximum System Voltage V_{SYS}	[V]	1000 (IEC) / 600 (UL 1703)	**Safety Class**	II
Maximum Reverse Current I_R	[A]	5.1	**Fire Rating**	C
Wind/Snow Load	[Pa]	5400	**Permitted module temperature on continous duty**	-40 °C up to +85 °C

QUALIFICATIONS AND CERTIFICATES

IEC 61646 (Ed. 2), IEC 61730 (Ed.1) application class A, UL 1703
The production site is certified according to ISO 9001 for Quality Management.

Safety Class II

C Certified US
UL 1703

The content of this data sheet is according to DIN EN 50380.

PARTNER

NOTE: Installation instructions must be followed. See the installation and operating manual or contact the technical service for further information on approved installation and use of this product.

Q-CELLS SE
OT Thalheim, Sonnenallee 17–21
06766 Bitterfeld-Wolfen, Germany

TEL +49 (0)3494 66 99-0
FAX +49 (0)3494 66 99-199

EMAIL service@q-cells.com
WEB www.q-cells.com

MSX120 Solar Panel from BP Solar

Electrical Characteristics	
STC Power Rating P_{mp} (W)	120
Open Circuit Voltage V_{oc} (V)	42.1
Short Circuit Current I_{sc} (A)	3.87
Voltage at Maximim Power V_{mp} (V)	33.7
Current at Maximim Power I_{mp} (A)	3.56
Panel Efficiency	10.9%
Fill Factor	73.7%
Power Tolerance	-3.00% ~ 3.00%
Maximum System Voltage V_{max} (V)	1000
Maximum Series Fuse Rating (A)	20
Temperature Coefficients	
Temperature Coefficiency of I_{sc}	0.065 %/ºC
Temperature Coefficiency of V_{oc}	-0.38 %/ºC
Temperature Coefficiency of P_{mp}	-0.50 %/ºC
Mechanical Characteristics	
Cell Type	Polycrystalline Cell
Cell Size(mm)	125 × 125
Cells	6 × 12
Dimensions	1108.0 × 991.0 × 50.0mm (39.0 × 43.6 × 2.0 inch)
Weight	13.0Kg (28.7 lbs)
Junction Box (Safety Rating, Bypass Diodes)	
Positive Cable (Length, Cable Cross-Section)	
Negative Cable (Length, Cable Cross-Section)	
Plug Connector (Type, Safety)	
Front Cover (Thickness,Material)	
Backsheet Cover (Color, Thickness, Material)	
Encapsulation Materials	
Frame Material	

Operation Conditions	
Nominal Operating Cell Temperature (NOCT)	47.0ºC
Operating Temperature	-40.0ºC to 85.0ºC
Maximum Load	5400
Hail Storm Rating	
Fire Safety Rating	
Warranty & Certification	
Certificates	• UL 1703 • CE Europe • IEC 61215 Ed.1 • IEC 61730 Ed.1
Defects & Workmanship Warranty Period	5.0 Years
90% Power Output Warranty Period	10.0 Years
80% Power Output Warranty Period	20.0 Years
Are Warranties Insured By Third Party	False

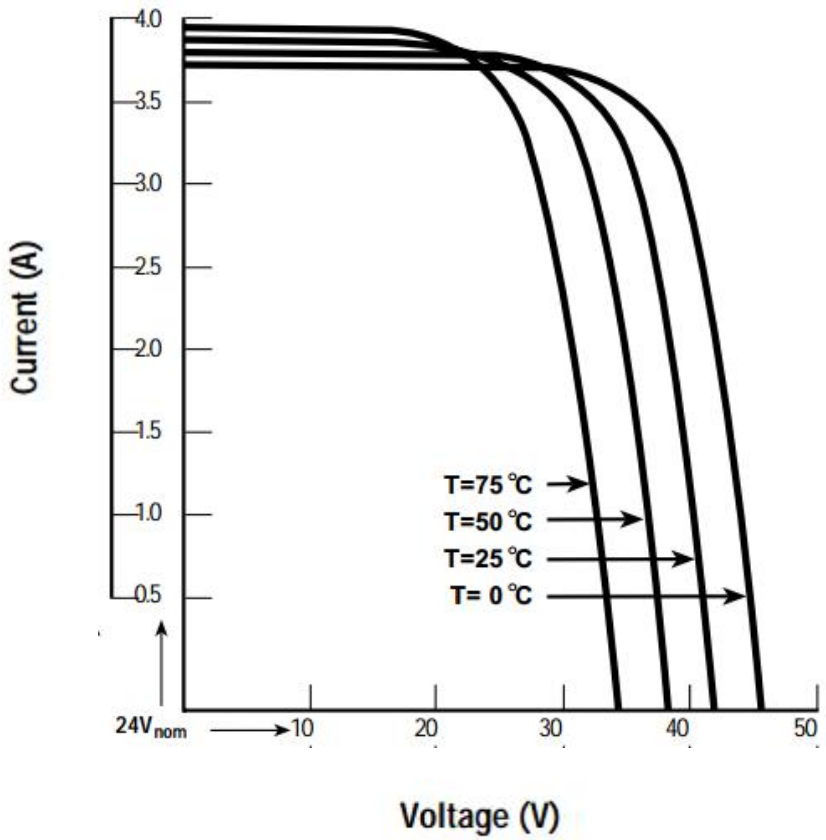

SPECIFICATION CATEGORIES		Db Mono	Kb Poly	Cb Mono	Lb Poly	Rb Poly	Rb Poly	Md Poly	Md Poly	Sb Poly	Sb Poly	Sb Poly	
		STP005B -12/DEA	STP010D -12/KEA	STP020B -12/CEA	STP030D -12/LEA	STP040D -12/REA	STP045D -12/REA	STP050D -12/MEA	STP055D -12/MEA	STP060D -12/SEA	STP065D -12/SEA	STP070D -12/SEA	
ELECTRICAL CHARACTERISTICS	Open-Circuit Voltage (Voc)	21.6 V	21.6 V	21.7 V	21.6 V	21.8 V	22.0 V	21.8 V	22.2 V	21.6 V	21.8 V	22.0 V	
	Optimum Operating Voltage (Vmp)	17.4 V	17.4 V	17.6 V	17.2 V	17.4 V	17.6 V	17.4 V	17.5 V	17.4 V	17.6 V	17.8 V	
	Short-Circuit Current (Isc)	0.32 A	0.65 A	1.26 A	1.94 A	2.58 A	2.79 A	3.13 A	3.34 A	3.90 A	4.11 A	4.27 A	
	Optimum Operating Current (Imp)	0.29 A	0.57 A	1.14 A	1.74 A	2.30 A	2.58 A	2.93 A	3.14 A	3.45 A	3.69 A	3.93 A	
	Maximum Power at STC (Pmax)	5 Wp	10 Wp	20 Wp	30 Wp	40 Wp	45 Wp	50 Wp	55 Wp	60 Wp	65 Wp	70 Wp	
	Operating Temperature	-40°C to +85°C	-40°C to +85°C	-40°C to +85°C	-40°C to +85°C	-40°C to +85°C	-40°C to +85°C	-40°C to +85°C	-40°C to +85°C	-40°C to +85°C	-40°C to +85°C	-40°C to +85°C	-40
	Maximum System Voltage	715 V DC	715 V DC	715 V DC	715 V DC	715 V DC	715 V DC	715 V DC	715 V DC	715 V DC	715 V DC	715 V DC	
	Maximum Series Fuse Rating	5 A	5 A	5 A	5 A	10 A	10 A	10 A	10 A	15 A	15 A	15 A	
	Power Tolerance	±10 %	±10 %	±10 %	±10 %	±5 %	±5 %	±5 %	±5 %	±5 %	±5 %	±5 %	
MECHANICAL CHARACTERISTICS	Solar Cell	Mono-crystalline solar cell	Poly-crystalline solar cell	Mono-crystalline solar cell	Poly-crystalline solar cell	Poly-crystalline solar cell	Poly-crystalline solar cell	Poly-crystalline solar cell	Poly-crystalline solar cell	Poly-crystalline solar cell	Poly-crystalline solar cell	Poly-crystalline solar cell	
	No. of Cells	36 (4×9)	36 (6×6)	36 (2×18)	36 (4×9)	36 (4×9)	36 (4×9)	36 (4×9)	36 (4×9)	36 (4×9)	36 (4×9)	36 (4×9)	
	Dimensions	216 × 306 × 18 mm	310 × 368 × 18 mm	656 × 306 × 18 mm	426 × 680 × 18 mm	537 × 665 × 30 mm	537 × 665 × 30 mm	631 × 665 × 30 mm	631 × 665 × 30 mm	771 × 665 × 30 mm	771 × 665 × 30 mm	771 × 665 × 30 mm	
	Weight	0.8 kgs	1.5 kgs	2.5 kgs	3.2 kgs	4.5 kgs	4.5 kgs	6.4 kgs	6.4 kgs	6.2 kgs	6.2 kgs	6.2 kgs	
	Junction Box	IP65 rated	IP65 rated	IP65 rated	IP65 rated	IP65 rated	IP65 rated	IP65 rated	IP65 rated	IP65 rated	IP65 rated	IP65 rated	
	Output Cables	(Optional cable available)	(Optional cable available)	(Optional cable available)	(Optional cable available)	(Optional cable available)	(Optional cable available)	(Optional cable available)	(Optional cable available)	H+S (12 AWG) Lengths: 750mm(-) and 750mm(+) Connection: MC Plug Type IV	H+S (12 AWG) Lengths: 750mm(-) and 750mm(+) Connection: MC Plug Type IV	H+S (12 AWG) Lengths: 750mm(-) and 750mm(+) Connection: MC Plug Type IV	H- an C
TEMP. CHARACTERISTICS	Nominal Operating Cell Temperature (NOCT)	45±2°C	45±2°C	45±2°C	45±2°C	45±2°C	45±2°C	45±2°C	45±2°C	45±2°C	45±2°C	45±2°C	
	Temp. coefficient of Pmax	-0.48 %/°C	-0.47 %/°C	-0.48 %/°C	-0.47 %/°C	-0.48 %/°C	-0.48 %/°C	-0.47 %/°C	-0.47 %/°C	-0.47 %/°C	-0.47 %/°C	-0.47 %/°C	
	Temp. coefficient of Voc	-0.34 %/°C	-0.34 %/°C	-0.34 %/°C	-0.34 %/°C	-0.34 %/°C	-0.34 %/°C	-0.34 %/°C	-0.34 %/°C	-0.34 %/°C	-0.34 %/°C	-0.34 %/°C	
	Temp. coefficient of Isc	0.037 %/°C	0.045 %/°C	0.037 %/°C	0.045 %/°C	0.037 %/°C	0.037 %/°C	0.045 %/°C	0.045 %/°C	0.045 %/°C	0.045 %/°C	0.045 %/°C	

Lb Poly STP030D-12/LEA

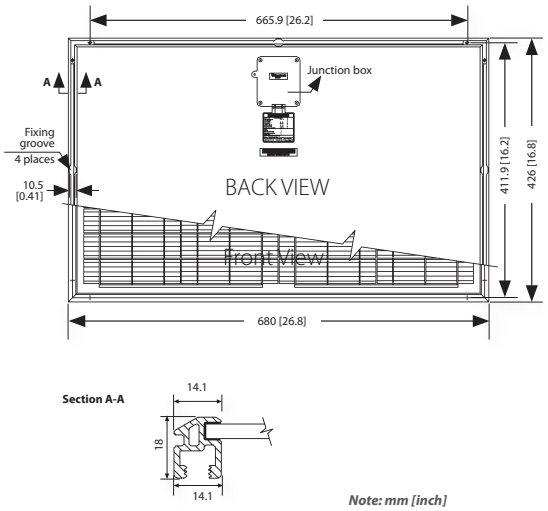

Note: mm [inch]

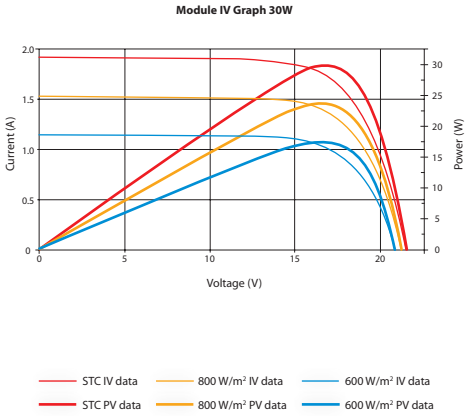

Rb Poly STP040D-12/REA

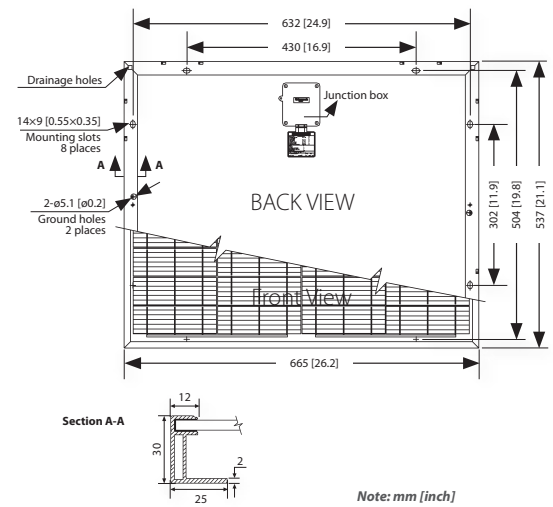

Note: mm [inch]

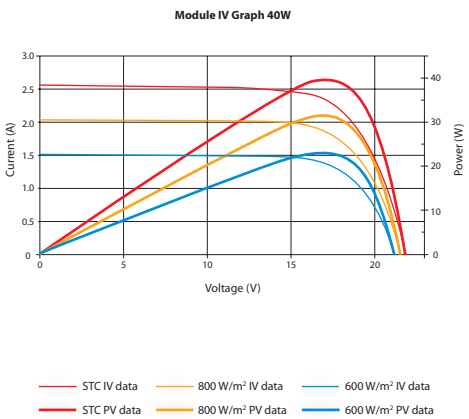

Md Poly STP050D-12/MEA

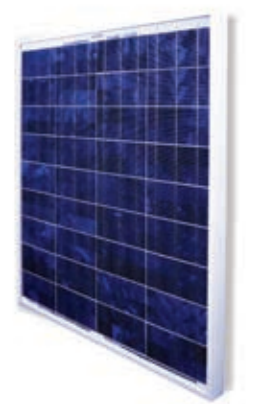

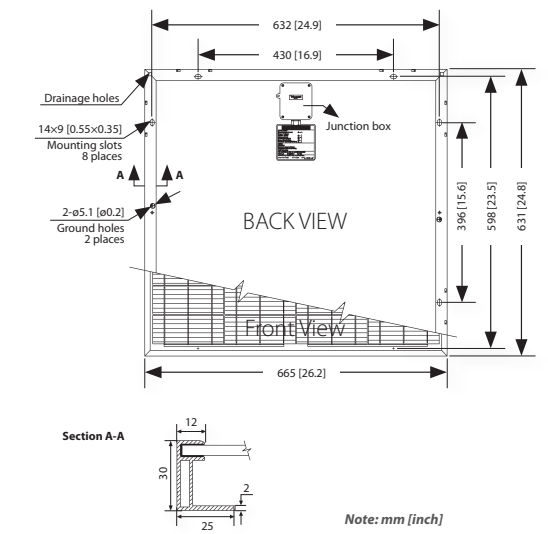

Note: mm [inch]